JOHANNES KEPLER
UNIVERSITÄT LINZ | JKU

TNF

Technisch-Naturwissenschaftliche
Fakultät

Electrical Characterization of Vertical Organic Transistors

DIPLOMARBEIT

zur Erlangung des akademischen Grades

Diplomingenieurin

im Diplomstudium

Technische Chemie

Eingereicht von:
Doris Sinwel

Angefertigt am:
Institut für physikalische Chemie

Beurteilung:
o. Univ. Prof. Dr. Serdar N. Sariciftci

Linz, 17. Februar 2011

Acknowledgements

First and foremost, I want to thank my family for all their support and motivation throughout the last 25 years and Dominik for his love and patience.

Furtheron, Prof. Sariciftci is thanked for enabling this work and Philipp Stadler for the supervision.

I am very grateful for Martin Egginger's help on experimental tasks and theoretical understanding and for introducing me to the topic of organic transistors. Robert Koeppe is thanked for his never-ending encouragement and his brave attempts to teach physics to a chemist.

Additionally, I would like to express my gratitude towards Sandra Kogler and Engelbert Portenkirchner for their help in the labs and the fruitful discussions.

I also want to thank all the members and visitors of the LIOS institute for their support and advice, Helmut Neugebauer, Alberto Montaigne Ramil, Almantas Pivirikas, Birgit Paulik, Christoph Ulbricht, Daniel Egbe, Elif Arici-Bogner, Eric Glowacki, Gebhard Matt, Gerda Kalab, Jacek Gasiorowski, Mamatimin Abbas, Manfred Lipp, Mateusz Bednorz, Matthew White, Mihai Irimia-Vladu, Patchanita Thamyongkit, Petra Neumaier, Stefan Schaur, Stefan Kraner, Valery Bliznyuk, Beatriz Meana-Esteban, Anita Fuchsbauer, Cigdem Yumusak, Serpil Tekoglu, Florian Kuhnlenz, Alessandra Operamolla and Sandro Lattante.

The SoMaP team, especially Melanie Reisinger, Oskar Armbruster, Josef Stadlbauer, Alexander Kogler and Richard Baumgartner, is thanked for the good collaboration and nice working atmosphere.

Thank you.

Eidesstattliche Erklärung

Ich erkläre an Eides statt, dass ich die vorliegende Diplomarbeit selbstständig und ohne fremde Hilfe verfasst, andere als die angegebenen Quellen und Hilfsmittel nicht benutzt bzw. die wörtlich oder sinngemäß entnommenen Stellen als solche kenntlich gemacht habe.

Linz, im Februar 2011

Doris Sinwel

Abstract

Vertical organic transistors exhibit high output currents in comparison to conventional organic field effect transistors and may be able to open new fields of applications. These vertical devices exhibit a simple geometry reminding strongly of the inorganic bipolar transistor. A small voltage applied to the base can modulate the charge carrier flux from the emitter to the collector which are sandwiching the base. Different working mechanisms are proposed depending on the nature of the base electrode. While the metal base transistor (MBT) is a hot-electron device comprising a very thin pinhole-free base layer with a working principle based on ballistic transport, the charge carriers move through openings in the base exhibiting a reduced energy barrier in case of the permeable metal base transistor (PBT). Detailed knowledge about the structure of the base electrode and the working mechanism is not only of theoretical interest, as it allows a well-aimed optimization of vertical transistors.

Proof of the concept of vertical organic transistors (VOTs) was reported in 1994 by Y. Yang and A. J. Heeger [1]. 2005, Fujimoto et al. [2] published devices incorporating buckminsterfullerene C_{60} and MePTCDI, which are reproduced in this work. Furtheron, the structure is simplified by using only one semiconductor material for both the emitter and the collector layer, which leads to a significant improvement in performance. The effect of the work function of the emitter metal on the electron injection is studied by use of different emitter materials. To investigate the base electrode in greater detail, atomic force microscopy (AFM) and scanning electron microscopy (SEM) measurements as well as additional electrical measurements are performed. The underlying collector layer exhibits a high roughness which leads to a higher surface area than the macroscopic area defined by the evaporation mask geometry, thus the predominant simplified imagination of the base electrode as flat sheet is falsified. Instead, a complex threedimensional nanomorphology, which is also affirmed by percolation measurements of aluminium on MePTCDI, is found for the modulating electrode.

Zusammenfassung

Vertikale organische Transistoren ermöglichen im Vergleich zu organischen Feldeffekt-Transistoren die Steuerung wesentlich höherer Ströme und können dadurch in Bereichen Anwendung finden, in denen bisher nur Elektronikbauteile basierend auf anorganischen Halbleitern eingesetzt werden konnten. Die bisher publizierten vertikalen organischen Transistoren ähneln einander in der Struktur, die der des anorganischen Bipolartransistors entspricht. Ein Strom zwischen Emitter und Kollektor wird durch ein dazwischen eingebettetes Base moduliert. Trotz ihres identischen Aufbaus werden die organischen Analoga anhand ihres Funktionsmechanismus in zwei Gruppen unterteilt. In Transistoren mit durchgehender Base-Elektrode müssen die Ladungsträger diese Elektrode in einem ballistischen Prozess durchdringen, um den Kollektor zu erreichen; man spricht von "metal base transistors" (MBTs). Ist die Base-Elektrode aber löchrig, können die Elektronen durch diese Öffnungen in die Kollektorschicht gelangen; es handelt sich dann um einen "permeable base transistor" (PBT). Das Wissen um die Art des vorherrschenden Ladungstransportes ist nicht nur von theoretischem Interesse, sondern auch von großer Bedeutung für die Optimierung von Transistoren, da deren Leistungsfähigkeit stark durch die Base-Elektrode beeinflusst wird.

In dieser Arbeit wird im ersten Schritt die Funktionsfähigkeit bereits publizierter vertikaler organischer Transistoren (VOTs), die Buckminsterfulleren C_{60} und ein Perylendiimidderivat (MePTCDI) als Halbleiter beinhalten, bestätigt. Spezifische Kennwerte und Reproduzierbarkeit können durch Verwendung von MePTCDI als Kollektor- und Emitterhalbleitermaterial deutlich verbessert werden. Anhand dieser modifizierten Transistoren wir der Einfluss der Arbeitsfunktion der Emitterelektrode durch Einsatz verschiedener Metalle untersucht. Um die Struktur der Base-Elektrode zu erforschen, werden bildgebende Verfahren, Rasterkraftmikroskopie und Elektronenmikroskopie, eingesetzt und elektrische Messungen durchgeführt. Dabei zeigt sich, dass die vorherrschende vereinfachte Betrachtung der Elektrode als glatte Fläche revidiert werden muss. Duch die große Rauigkeit der darunterliegenden Kollektorschicht ergibt sich stattdessen eine komplexe dreidimensionale Nanostruktur.

Contents

Part I

Introduction

1 Motivation

Organic electronics have proven to be a low-cost alternative to their inorganic counterparts and show promising advantages such as use in flexible displays and RFID tags, simplification of production processes etc. In case of organic transistors, their application in diverse fields requiring high output currents, e. g. to drive LEDs, might be realized by the use of vertical devices. In contrast to the organic field effect transistor, the charge carriers move in the case of the organic vertical transistor through the device perpendicularly to the substrate and thus have to travel distances of less than a micron.

Many inorganic devices exhibit a vertical geometry, therefore diverse attempts have been made to transfer their structure to organic electronics. The modulation of a current between two separated electrodes by the use of a third electrode placed inbetween was first reported in 1907 when E. Lilienfeld patented the vacuum tube. 40 years later the bipolar transistor was invented in the Bell Laboratories, the vertical concept was applied successfully in semiconductor technology. The replacement of the semiconducting base by a metal base electrode resulted in the semiconductor-metal-semiconductor transistor. Its hybrid variations incorporate one inorganic and one organic semiconductor layer, thus they form a link between inorganic and organic vertical transistors. The latter contain two organic semiconducting layers sandwiching a metal base and have been proven to work with a wide variety of organic materials.

As devices incorporating C_{60} and MePTCDI show very promising results, they are investigated in detail in this work. After reproduction summarized in chapter 6, the different components are investigated separately. The importance of the correlation of the work functions of the semiconducting emitter and collector materials is examined by deposition of MePTCDI as both emitter and collector layer. The electron injection from the emitter electrode into the collector semiconducting layer is investigated for several electrode materials exhibiting different work functions in chapter 8. As the base electrode is known to be of crucial importance, its morphology and the influence of the deposition geometry are discussed separately in chapter 9. Both the underlying collector layer, which serves as a substrate for the base evaporation, and the base electrode itself are subjected to imaging techniques, namely AFM and SEM. To confirm the obtained results concerning surface roughness, a percolation measurement is carried out. A heat treatment of the aluminium base electrode in air is known to affect the device performance positively as shown in chapter 7, thus it is investigated by a simultanous resistance measurement.

2 Vertical Transistors

2.1 Vacuum tube

In 1907, the first three-terminal device comprising three metal electrodes in a low vacuum glass tube was patented by Lee de Forest as detector of electromagnetic waves under the name "Audion" [3]. From 1911 on, the triode was used as amplifier, although the working mechanism was figured out only years later by Langmuir.

2.1.1 Working principle:

Ejection of electrons by a metal can be achieved in different ways such as thermionic emission or secondary emission due to bombardment with electrons. Additionally, the ejection can be induced by light (photoeffect) or by application of a high electric field between the metal and a counter electrode (field-induced emission) or bombardment with positive ions [4]. As thermionic emission leads to electron ejection in case of triodes, it will be discussed in the following.

A negative space-charge cloud in close vicinity of the heated metal is formed which counteracts further emission, an equilibrium is established. The saturation current density J from a heated metal is given by the Richardson-Dushman equation and depends exponentially on temperature [5]:

$$J = A * T^2 * e^{-\frac{\phi}{kT}} \tag{2.1}$$

The absolute temperature is abbreviated with T, the Boltzmann constant with k. ϕ stands for the work function of the material which gives the energy needed to lift an electron from ground state to vacuum. A is an experimental factor depending on the material. While for the first devices metals like tantalum and tungsten were used as cathodes, platinum filaments covered with metal oxides were developed to optimize the experimental factors (lowering of the work function, increase of A) and to gain the same thermionic emission for a lower temperature.

For a thermionic emitter biased negatively with respect to its surroundings, the resulting electric field lowers the work function of the metal by an amount of $\Delta\phi$ which is directly proportional to the square root of the applied field. This field enhanced thermionic emission (Schottky effect) results in the following equation:

$$J = A * T^2 * e^{-\frac{(\phi-\Delta\phi)}{kT}} \tag{2.2}$$

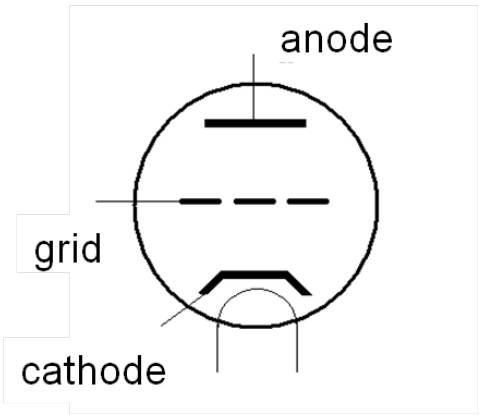

Figure 2.1: Vacuum tube. The electron flux from the heated cathode to the anode is modulated by the grid.

If now the positively biased electrode, the anode, is put close to the system, it attracts electrons from the space-charge cloud, current is flowing. The electron cloud near the cathode lowers the potential between cathode and anode by shielding of the positive voltage. Thus, the current is space charge controlled and will only saturate for very high voltages, when all emitted electrons are attracted by the anode. For the space charge region, the Langmuir-Child law, also known as Langmuir-Schottky law, can be applied to obtain the space charge limited current [4, 5]:

$$I = const * V_a^{\frac{3}{2}} \tag{2.3}$$

The term *const* contains the distance between the electrodes and the area, the voltage applied at the anode is denoted as V_a.

The electron flux from the cathode to the anode can be modulated by the insertion of a biased metal grid, as shown in fig. 2.1.

Negative charge on the grid repels the electrons from the cathode, thereby decreasing the output current. Fig. 2.2 shows this effect for gate voltages from -1 to -9 V. At the pinch-off voltage no electron flux to the anode is possible. Positive charge on the grid, on the other hand, accelerates the electrons towards the anode and yields higher anode current although it draws some electrons from the vacuum and thereby leads to a grid current. The increase in anode current is depicted in fig 2.2 for gate voltages from 1 to 3 V. The anode current depends both on the grid voltage and the anode voltage.

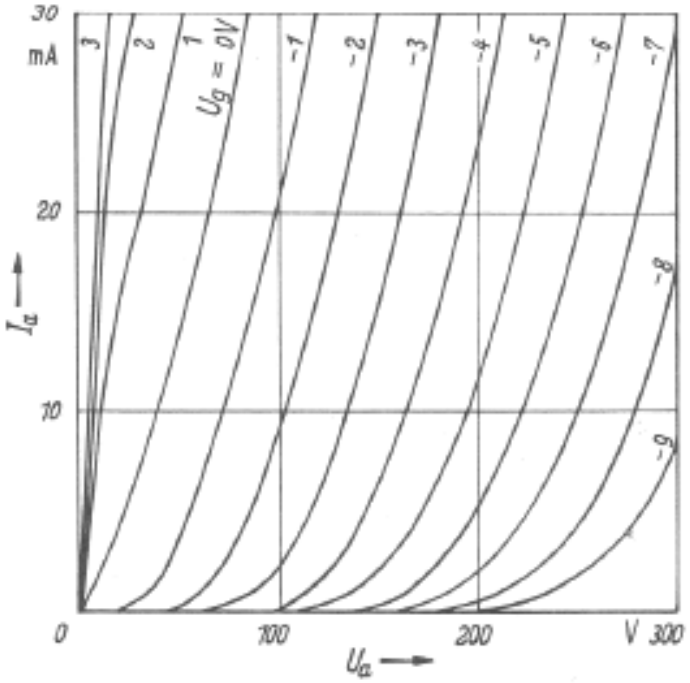

Figure 2.2: Current-voltage characteristics of a vacuum tube, amplification is observed for positive grid voltage, decrease at negative grid voltage. [6]

2.2 Transistors based on semiconducting materials

1944, 120 years after J. Berzelius' discovery of elementary silicium, the first patent on silicium doping was filed by John Robert Woodward. Only three years later, the pn junction was discovered by W. Shockley, W. Brattain and J. Bardeen. Deeper understanding soon led to the invention of the bipolar transistor; the junction between metal and semiconductor was the basis for the inorganic metal base transistor, which served as model for several devices comprisig organic materials.

2.2.1 p-n junction

In this chapter, the ideal case of a p-n junction, the abrupt junction, is considered. This junction is based on the assumption that the dopant atoms in the semiconductor change abruptly from n-type to p-type [7, 8]. At the interface, both electrons from the n-type and holes from the p-type semiconductor diffuse into the opposite part of the junction due to the large carrier concentration gradient. Thus, both regions near the interface are depleted of free charge carriers (depletion region, space-charge region) but at the same time their counter ions appear as fixed charge centers. In a first approximation, the space-charge distribution can be assumed as box-like. The box size depends on the dopant concentration - the higher the concentration, the narrower is the depletion width. In fig. 2.3, the boxe-like space charge areas are shown for a p-n junction comprising a highly doped p-type and a less doped n-type semiconductor.

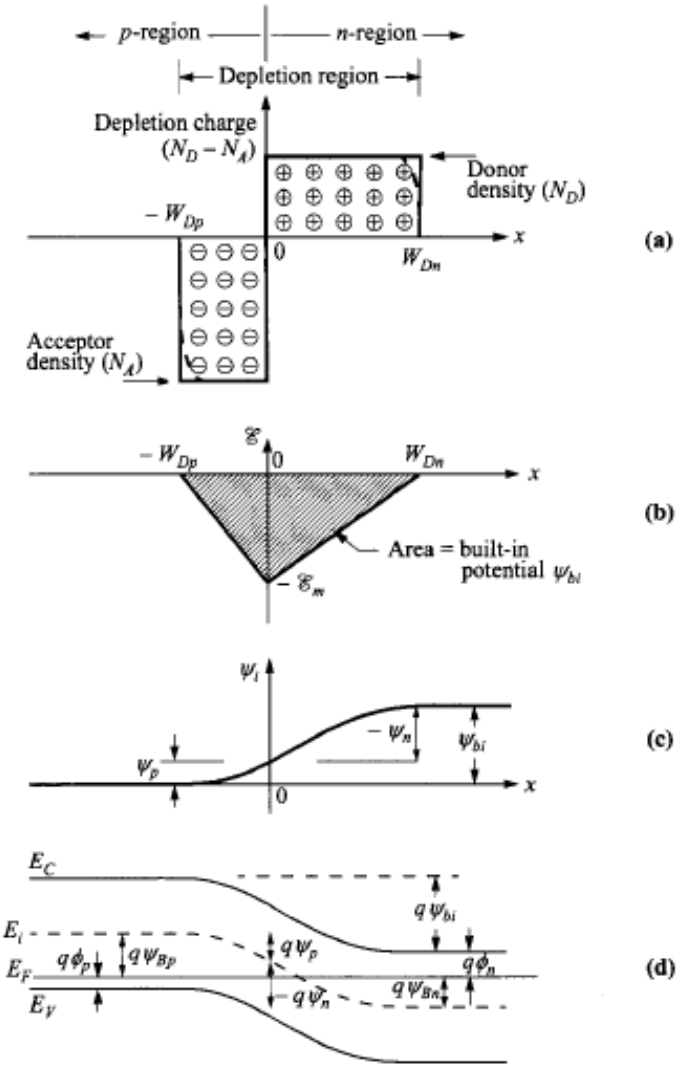

Figure 2.3: p-n junction. (a) space charge distribution in box-like approximation, the dashed line marking the correct distribution. (b) Electric field built up by the space charge. (c) Potential distribution throughout the junction. (d) Energy diagram.

This charge separation leads to an electric field in the depletion region counteracting further diffusion, thereby establishing an equilibrium at a fixed temperature as depicted in sketch (b) in fig. 2.3. The electric field exhibits a maximum directly at the interface, decreasing linearly. Integration gives the built-in potential ψ_{bi}, which is the potential difference from the electroneutral n-type to the electroneutral p-type semiconductor outside the depletion region. In the energy-band diagram the built-in potential is found in the energy difference between the conduction band edges. In equilibrium, the Fermi level is constant throughout the junction, as no net current is flowing (fig. 2.3 (d)).

When a voltage is applied to the p-n junction, the equilibrium between diffusion current due to the charge carrier gradient and the drift current due to the electric field is affected.

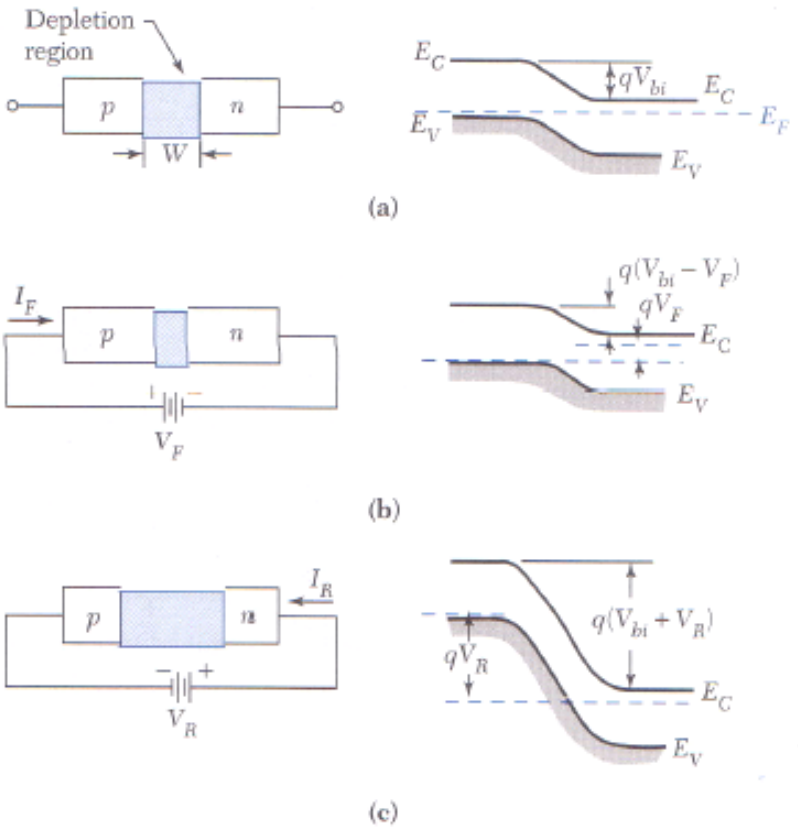

Figure 2.4: pn-junction, (a) not biased, (b) forward and (c) reverse biased.

2.2.1.1 Forward bias: To reduce the depletion width, the n-type semiconductor is biased negatively with respect to the p-type semiconductor. The majority carriers of each component are repelled by the bias and pushed towards the interface as depicted in fig. 2.4. As the space-charge region gets narrower, the electric field is lowered until the charge carriers can cross the interface. Once in the differently doped counterpart, they appear as minority carriers and recombine within a short distance, the diffusion length. The current increases rapidly with the applied voltage.

2.2.1.2 Reverse bias: When the diode is biased oppositely, the depletion width and the electric field across the junction increase with the applied voltage, no current flows initially (fig. 2.4 (c)). At a critical voltage (breakdown voltage), the current increases suddenly, the pn-junction gets conducting. The three most important breakdown mechanisms are discussed in the following [7, 8]:

2.2.1.2.1 Thermal instability: When a reverse bias is applied, a small reverse current of minority charge carriers flows through the junction and leads to heat dissipation. At a threshold voltage, the temperature rise leads to a thermal runaway, the device is destroyed [9]. While the thermal runaway is of great importance at room temperature, other mechanisms can induce the breakdown at low temperatures, too.

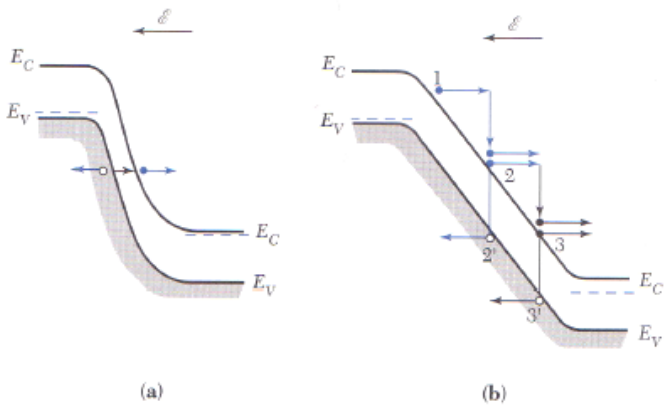

Figure 2.5: (a) Tunneling and (b) Avalanche multiplication

2.2.1.2.2 Tunneling effect: At a high electric field and a high doping concentration, a valence electron can change from the valence band to the conduction band by tunneling (fig. 2.5 (a)). The breakdown voltage decreases with increasing temperature.

From the classical mathematical point of view, the probability to cross the junction is zero for an electron with an energy lower than the potential barrier. For the quantum-mechanical calculation, there is a small probability to find a valence electron from the p-type part of the junction in the n-type part which discribes the tunneling effect.

2.2.1.2.3 Avalanche Multiplication: If a sufficiently high electric field is applied, it accelerates thermally generated electrons in the depletion region, these charge carriers gain kinetic energy as the distance they travel increases. While an electron moves through the depletion layer, it can be scattered by a phonon (vibrating crystal atom) or an impurity atom. At this collision, an electron-hole pair may be created. These newly formed charge carriers can again be accelerated and give rise to following collisions. As the distance between two collisions (scattering length) is much smaller than the depletion width, a high number of free charge carriers can be generated as depicted in fig. 2.5 (b).

At increasing temperature, phonon scattering is enhanced, the scattering length decreases. Thus, the electrons have to gather the kinetic energy they need to create the next electron-hole pair within a shorter distance. To achieve this, the electric field which accelerates the electrons has to be increased. In short, increasing temperature increases the breakdown voltage, the temperature coefficient is positive.

This avalanche multiplication gices rise to a hysteresis in the current-voltage characteristics, high current is still observed after lowering the voltage below the breakdown voltage.

2.2.2 n-p-n and p-n-p Junction: The Bipolar Transistor

The bipolar transistor was invented 1947 in the Bell Laboratories and soon replaced the triode as amplifier and switching device. Instead of three electrodes separated by vacuum, the bipolar transistor consists of three layers of alternately doped semiconductors, thus comprising two contacts between n- and p-type semiconductors as described in the previous chapter.

2.2.2.1 Working principle of the bipolar transistor The bipolar transistor consists of three alternating layers of differently doped semiconductors, namely n-p-n or p-n-p, of which only the first one will be discussed here. The very thin p-doped base is sandwiched between the emitter and the collector which are both n-doped as it is depicted in fig. 2.6. As described previously, in the non-biased state depletion layers are formed.

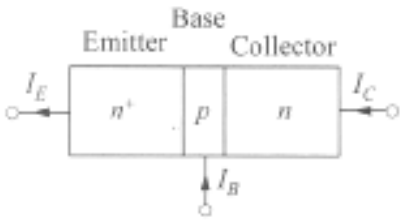

Figure 2.6: npn-transistor, taken from [8].

When connecting the transistor, the three circuit configurations common-emitter, common-base and common-collector can be applied as shown in fig. 2.7.

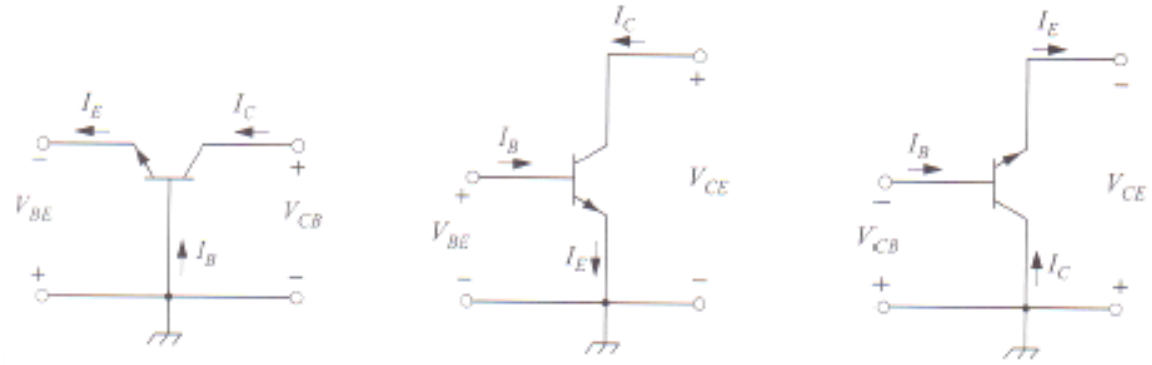

Figure 2.7: Circuit configurations for a bipolar transistor, common-base (left), common-emmiter (middle) and common-collector (right), fig. taken from [8].

In the common-emitter circuit, the emitter is grounded, and when a positive collector voltage is applied with respect to the emitter, the base-emitter diode is forward biased, but the collector-base diode is reverse biased. No electrons from the emitter can reach the collector. At application of an additional positive base voltage the base-emitter diode gets conducting, electrons are injected into

the depleted base electrode. Because of the potential drop, a large part of the electrons drifts to the collector.

Application of a forward bias to the emitter-base junction results both in injection of electrons from the emitter into the base and injection of holes from the base into the collector layer. While the total collector current is given by the sum of these contributions, only the electron current can give rise to the obtained collector current. Therefore, a high electron contribution and a low hole contribution to the emitter current are desirable. As the currents depend on the respective majority carrier concentrations, the doping concentration of the emitter is chosen higher than the doping concentration of the base.

To characterize a bipolar transistor, two types of measurement are carried out, yielding the output chracteristics and the transfer characteristics.

2.2.2.1.1 Transfer characteristics : This type of measurement is in case of common-emitter mode obtained by recording the collector current in dependence of the base voltage at a fixed collector voltage or collector current.

2.2.2.1.2 Output characteristics: When this type of measurement is carried out in common-emitter mode, the collector current is measured as function of the collector voltage for different constant base voltages or base currents. A set of graphs resembling fig. 2.9 is obtained.

2.2.2.2 Modes of operation The bipolar transistor can work as current amplifier, voltage-controlled current source or switch depending on the mode of operation. These four modes are descibed for a npn-transistor in this chapter on basis of the output characteristics and are depicted in fig. 2.8 [7].

Operation mode	Emitter-base bias	Collector-base bias
Normal, Active	Forward	Reverse
Saturation	Forward	Forward
Cutoff	Reverse	Reverse
Inverse	Reverse	Forward

Figure 2.8: Modes of operation, fig. taken from [8].

2.2.2.2.1 Cutoff Mode: In the cutoff mode, both junctions are reverse biased ($V_{eb} < 0$, $V_{cb} < 0$). In fig. 2.9, the cutoff mode is depicted as grey area.

2.2.2.2.2 Normal Active Mode: A base voltage is applied, the base-emitter junction is forward biased ($V_{eb} > 0$) and electrons from the emitter are injected into the base. These electrons are only sufficiently collected by the collector if the collector-base junction is reverse biased ($V_{cb} < 0$). In this case, the transistor is operating in the normal active mode between the saturation and the cutoff mode (both marked in grey) in fig. 2.9.

2.2.2.2.3 Saturation Mode: For small collector voltages, both the emitter-base junction and the collector-base junction forward biased ($V_{eb} > 0$, $V_{cb} > 0$). Electrons from the emitter are collected to a big part by the base, a reduced collector current is observed which does not increase with the base voltage. As depicted in fig. 2.9 for the grey area, the applied collector voltage in the saturation mode is very small while the collector current is increased significantly in comparison to the cutoff mode.

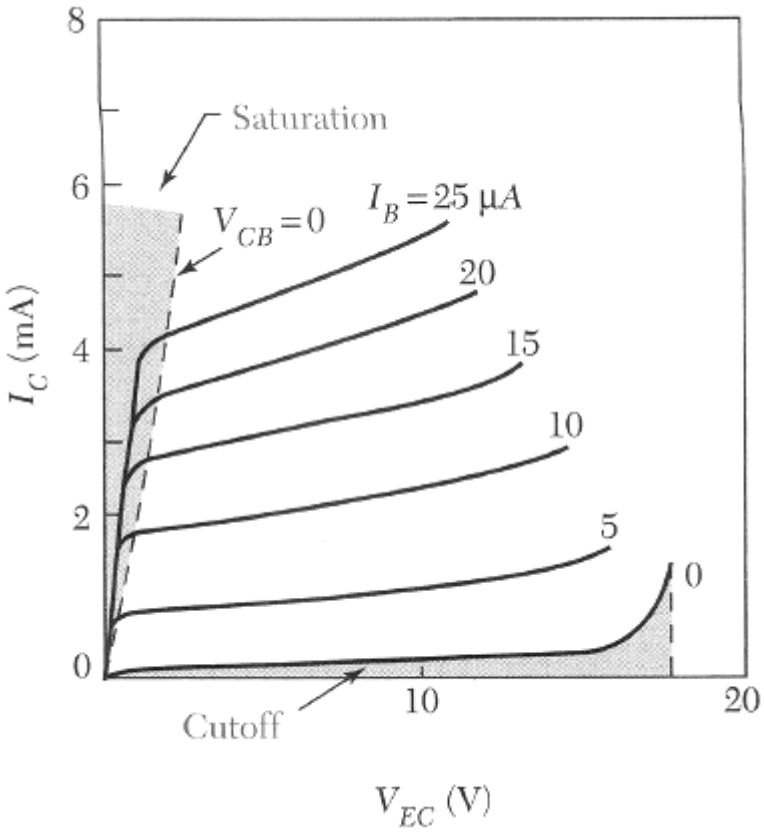

Figure 2.9: Saturation (4), cutoff (1), normal active mode (2) and (3) of a bipolar transistor, fig taken from [7].

2.2.2.2.4 Inverse Active Mode: In this case, both junctions are biased oppositely to the way they are biased in normal active mode. Electrons are emitted from the collector into the forward biased collector-base junction ($V_{cb} > 0$) and collected by the emitter after passing the reverse biased base-emitter junction ($V_{eb} < 0$). For a symmetrical npn structure, the inverse active mode is identical to the normal active mode, just swapping collector and emitter. For different doping levels of collector and emitter, the perfomance changes.

2.2.2.3 Applications of the bipolar transistor: As mentioned earlier, the bipolar transistor can be used as switch, current amplifier or voltage-controlled current source dependent on the operation mode.

Switch: To use a bipolar transistor as a switch, the operating points are chosen in the cutoff and the saturation mode, marked as grey areas in fig. 2.9. In the cutoff mode, the collector current is close to zero for any collector voltage. In saturation mode, a significant collector current is obtained for applied base voltage and very small collector voltage. Changing beween these operating modes, the transistor works as voltage-controlled switch, which is logically closed in saturation mode and open in cutoff mode.

An important parameter to rate the performance of a switch is the on/off ratio which can be obtained from the transfer characteristics. The on/off ratio is calculated from the collector current at applied base voltage devided by the collector current at zero base voltage (off-current, leakage current):

$$on/off = \frac{I_c(V_b \neq 0)}{I_c(V_b = 0)} = \frac{I_{c,on}}{I_{c,off}} \tag{2.4}$$

Voltage-contolled current source: In normal active mode, the application of a base voltage results in the output of a collector current which is over a wide range of the collector voltage only dependent on the chosen base voltage. Thus, the device works as a current source which is controlled by the base voltage. In the common-emitter output characteristics depicted in fig. 2.9 (2) and (3) indicate possible operating points for two different base voltages.

Current amplifier: Bipolar transistors working in normal active mode are also widely used as current amplifiers. The working principle is similar to the one of the voltage-controlled current source, but the amplifier works current-controlled. In common-emitter mode, a small base input current gives rise to the amplified output current at the collector.

To rate the performance of an amplifier, the current enhancement is of interest. The current enhancement factor β is calculated the following way [8]:

$$\beta = \frac{I_c}{I_b} \tag{2.5}$$

Thus, β gives the ratio of the amplified output current at the collector to the base current. The calculation is done similarly for common-base mode, here the common-base current enhancement factor α is obtained as the ratio of collector and emitter current:

$$\alpha = \frac{I_c}{I_e} = \frac{\beta}{1+\beta} \tag{2.6}$$

2.2.3 Metal-semiconductor contact: Schottky-junction

Junctions between metal and semiconductor appear in the classic MBT and the organic transistors prepared for this work, yet the difference between inorganic and organic semiconductor has to be taken into account. In this chapter, only the contact between inorganic semiconductor and metal is discussed.

The rectifying effect of metal-semiconductor junctions is known since 1874, leading to the use of point-contact rectifyers. The transport theory of semiconductors led to further understanding as it could be applied to m-s contacts. 1938, both Schottky and Mott published theoretical models on the observed barrier, which were followed by the theory on thermionic emission.

To understand what happens at the interface of a m-s junction, the first step ist to visualize the energy levels of the separated components as depicted in (a) in fig. 2.10 [8]. For the metal, the energy difference between the Fermi level and the vacuum level is defined as the metal's work function $q\phi_m$. In an n-type semiconductor, the Fermi level is situated between valence and conduction band, separated from the latter's edge by an energy difference of $q\phi_n$. The energy needed to reach the vacuum level from the conduction band edge is smaller than the metal's work function and given by the electron affinity $q\chi$. To calculate the semiconductor's work function defined as the energy difference between Fermi level and vacuum level, these two parts are added up to:

$$q\left(\chi + \phi_n\right)$$

When connecting the two components by a wire ((b) in fig. 2.10), electrons will flow from the semiconductor to the metal until the semiconductor's Fermi level is lowered to the metal's one, thereby being reduced by the following amount:

$$q\left[\phi_m - (\chi + \phi_n)\right]$$

The term in the square brackets is denoted as the contact potential.

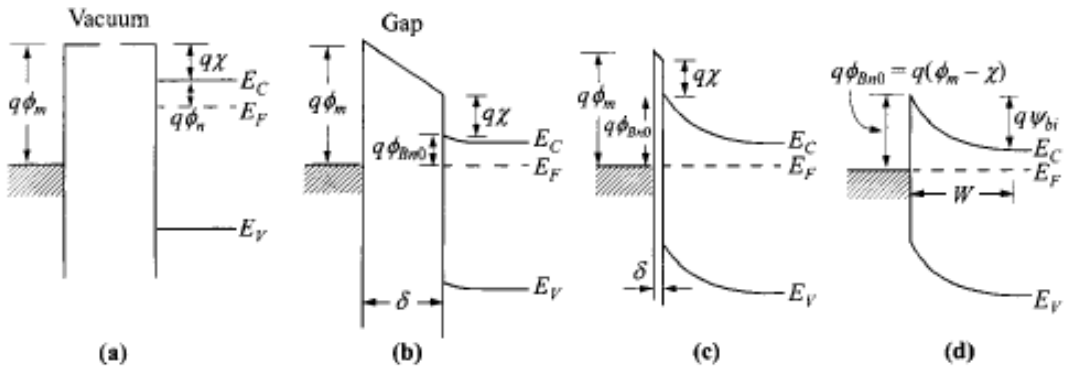

Figure 2.10: Schottky junction. (a)Metal and semiconductor not connected, (b) connected, (c) with small gap, (d) without gap.

To model an ideal contact between metal and semiconductor, their distance δ is reduced ((c) in fig. 2.10), thereby increasing the electric field until the positively charged depletion region of the semiconductor is touching the negatively charged metal surface. As the electron affinity $q\chi$ does not change in this process, the semiconductor's energy bands get bent up in the depletion region, creating a barrier height from the Fermi level to the band at the interface which is equal to the difference of the metal's and the semiconductor's work functions:

$$q\phi_{Bn0} = q\left(\phi_m - \chi\right) \tag{2.7}$$

The formed depletion region resembles the one of a pn-junction with a heavily doped p-semiconductor having a depletion width of 0 as shown in (d) in fig. 2.10.

Thus far, the s-m junction has been cosidered in thermal equilibrium, now the effects of forward and reverse bias are discussed. By applying forward bias V_F to the system (positive voltage between metal and semiconductor), electrons are pumped into the positively charged semiconductor. Apart from being emitted into the metal over the barrier which is lowered by qV_F (Schottky-diode), the electrons can overcome the barrier by quantum-mechanical tunneling (ohmic contact).

Once the electrons reach the metal, they do not appear as minority carriers because of the large number of free valence electrons being present in the metal. Thus, the accumulation of minority carriers and the resulting stored-charge-effects observed in the p-n junction is negligible in the m-s junction. This leads to faster responses to voltage changes.

On the other hand, application of reverse bias V_R (negative voltage between metal and semiconductor), increases the barrier height by qV_R, electrons from the semiconductor cannot pass the contact. The electrons from the metal still have to overcome the same potential barrier as before, $q\phi_m$, and give rise to the reverse-bias current.

2.2.4 Metal Base Transistor

In 1928, Julius E. Lilienfeld applied for a patent on the amplification of current in a semiconductor-metal-semiconductor structure, consisting of a metal layer sandwiched between two layers of e.g. copper sulfide [10]. The drawing depicted in fig. 2.11 is taken from this patent.

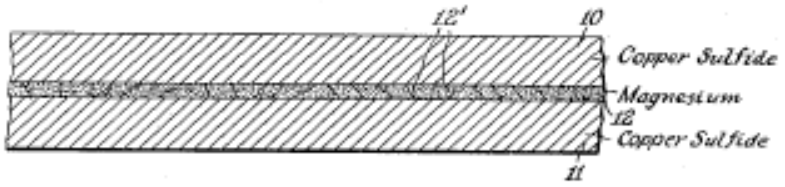

Figure 2.11: Lilienfeld's schematic drawing of the first current amplifier, (10) and (11) marking the semiconductors, (12) the metal layer, taken from [10].

34 years later, this structure was rebuilt using doped silicium as semiconductor; Atalla and Kahng proposed the metal-base transistor (MBT) for high-speed applications [11]. Yet, difficult preparation of the transistors and poor device parameters in terms of current amplification and leakage current prevented practical application.

The metal base transistor (MBT) consists of two identically doped silicium layers sandwiching a metal layer, the structure resembles the bipolar transistor, exchanging the base by an inserted metal. The MBT is defined as a hot-electron device. This means that the electrons have to enter the middle electrode and to cross it by ballistic transport. While in the bipolar transistor only a small part of the electrons flows through the depleted base electrode, the biased metal base electrode allows a higher base current leading to a small emitter collector transfer ratio.

Recombination, an obvious limiting factor of the electron transport through the base, depends on the ratio of the layer thickness and the mean free path for electrons in the metal. Apart from crossing the base metal, the electrons also have to overcome two interfaces (emitter-base and base-collector). For identical barrier heights at the interfaces in the energy diagram, quantum-mechanical reflection prohibits any electron transfer. Backscattering within the collector layer further decreases the emitter collector transfer ratio. [12]

The current enhancement factors for common-base and common-emitter mode are calculated as for the bipolar transistor (see eq. 2.6 and 2.5).

2.2.4.1 Permeable Metal Base Transistor Like the MBT, the permeable metal base transistor PBT is a majority carrier device. Electrons are transferred from emitter to collector mainly through pinholes in the base electrode beside the ballistic process known from the MBT. The base resembles a biased grating, the energy barrier is locally reduced at the openings. These holes can

vary in size and distribution, depending on production and used materials.

As current through openings and hot electrons add up to the collector current, the problem of defining these two contributions arises. 1986, Rasencher et al. reported a way of obtaining the pinhole contribution in devices sandwiching a $CoSi_2$ layer between two layers of n-doped silicium [13]: If the base is continuous, it shields the emitter from the electric field which is generated by application of a collector voltage V_{CB} and no change of emitter current I_E is observed. Thus, the following equation is only valid for a MBT with a continuous base:

$$\frac{\delta I_E}{\delta V_{CB}} = 0 \tag{2.8}$$

2.2.4.2 Inorganic-organic hybrid-transistors: In 2004, the concept of the metal base transistor was partly transferred to organic electronics by changing the emitter to an organic semiconductor. Considering the physical properties of the interface, the difference between inorganic and organic semiconductors has to be taken into account. The Schottky-contact described previously cannot be transferred to organic semiconductors without corrections.

2.2.4.2.1 Metal-organic interfaces: In an unbiased junction of metal and inorganic semiconductor, the vacuum level of the metal and the semiconductor is constant across the interface. In case of organic materials, the vacuum level of the semiconductor can be shifted because of an interface dipole induced by charge transfer between metal and semiconductor, lowering of the metal work function by adsorption of the organic material, population of metal-induced new energy levels within the gap at the interface, etc. [14]

Taking these possibilities into account, injection mechanisms different from overcoming the potential barrier can be postulated. The additional energy levels may allow charge carriers to pass the barrier by a hopping process through the midgap states. When applying a high electric field, charge carriers can also cross the barrier by tunneling as discussed in chapter 2.2.3.

2.2.4.2.2 Hybrid transistors - state of the art: Hybrid devices with emitters of C_{60}, tris(8-hydroxyquinoline) aluminium Alq_3 [15] and the p-type material N,N- diphenyl-N,N-bis(1-naphthylphenyl)-1,1-biphenyl -4 ,4- diamine (NPB), using n-doped or p-doped silicium, respectively, as collector layer are reported. Equ. 2.8 is not valid when applied to the measured data, so the devices are considered as PBTs although in atomic force microscope (AFM) measurements no holes can be observed. Therefore, the authors attribute the formation of pinholes to the oxidation processes during exposure to air at elevated or room temperature. This oxidation significantly increases reproducibility and performance of the devices.

Transfer and output characteristics are measured in common-emitter mode for different constant

collector and base current, and in common-base mode for different constant emitter and collector currents, respectively. As high off-current (leakage current) is observed, the calculation of the current amplification factor is modified. The off-current is substracted from the collector current before dividing it by the constant base current [16]:

$$\beta = \frac{I_c - I_{c.off}}{I_b} \tag{2.9}$$

Many modifications of the base electrode are published, e. g. using a conducting polymer blend as organic base material [17], which allows a high base transmission. Deposition and heating in air of a multilayered base consisting of Al and Ca [16] is assumed to lead to pinholes due to oxidation, a decrease in bse current is observed. An Al:Au base in combination with n-doped silicium and Alq_3 improves the semiconductor-metal contacts and thus the device performance [15].

2.2.4.3 Vertical organic transistors The concept of the permeable base transistor was already transferred successfully to the field of organic electronics in 1994 by Y. Yang and A. J. Heeger [1]. Spincoated layers of poly(2-methoxy-5-(2'-ethyl-hexyloxy)-1,4-phenylene vinylene (MEH-PPV) form the collector and emitter layer, while the metallic polymer PANI-CSA (polyaniline protonated with camphor sulphonic acid), which is known to self-assemble into a conducting network, serves as base electrode. When the insulating blend polymer (polyester resin of low molecular mass) is etched selectively, this porous and rough network remains, offering a high surface area and an inhomogenious electric field at application of a voltage. As the devices do not work at high PANI-CSA concentrations, the special network-like nanomorpology is assumed to be essential to the working mechanism.

Similar conclusions are drawn by Y. C. Chao et al. from the investigation of organic vertical transistors incorporating a metal grid between two layers of poly(3-hexylthiophene) P3HT [18]. The overlap of emitter and collector electrode defines an active area of 1 mm^2. The grid is manufactured by spincasting of a ethanolic solution of polystyrene spheres prior to the aluminium base evaporation of 30 nm. After the deposition, the spheres are removed with ethanol in an ultrasonic bath, leaving round openings in the electrode as shown in fig. 2.12. Thus, an inhomogenious network-like base electrode like the PANI-CSA electrode is formed. Charge carriers are assumed to cross the base electrode by traveling through the openings.

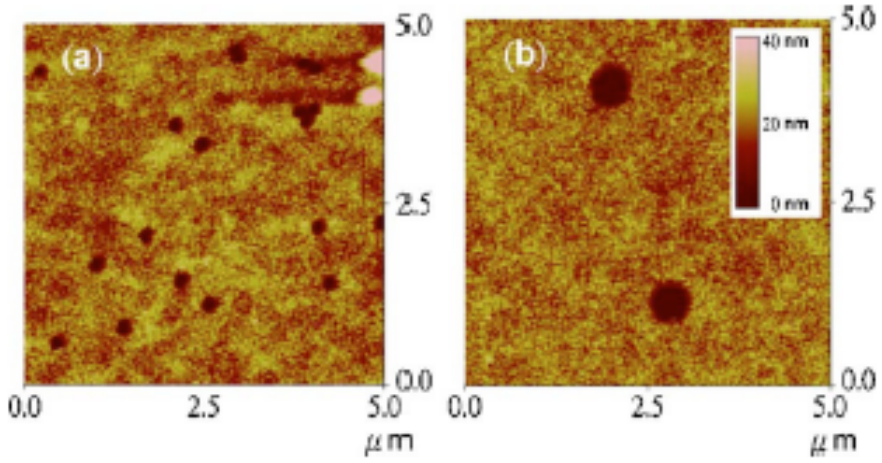

Figure 2.12: Grid electrode formed by spincasting of polystyrene spheres prior to the metal evaporation, taken from [18].

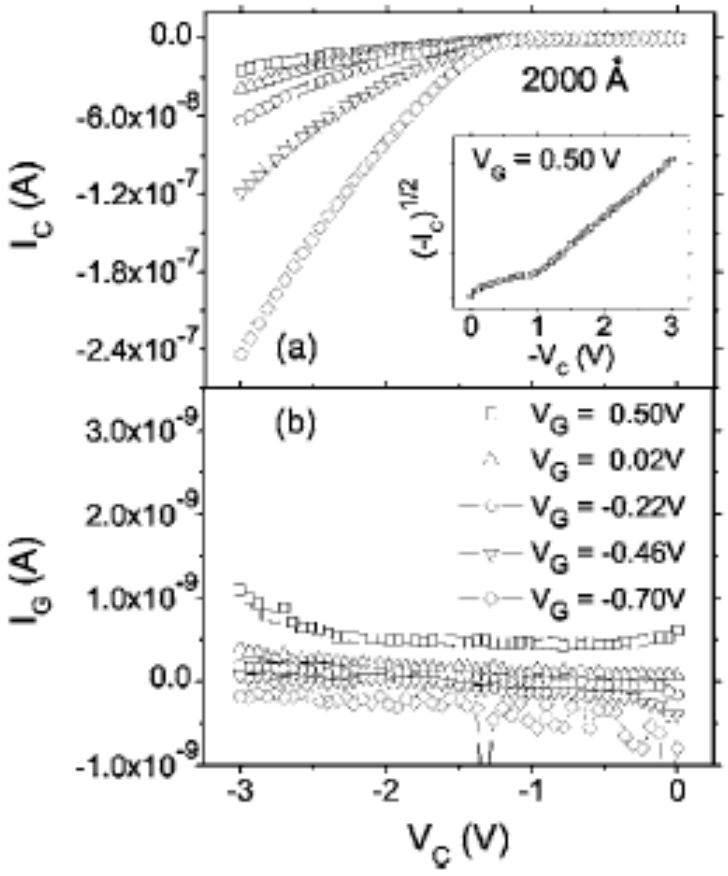

Figure 2.13: Output characteristics of a device containing a grid electrode, taken from [18].(a) Collector current vs. collector voltage, (b) base current vs. collector voltage.

At an operating voltage of 3 V, the devices reach a maximum current enhancement factor of 506; the maximum resulting collector current is found to be around 0.03 mA cm^{-2}. An output characteristics is shown in fig. 2.13.

In 2008, Hümmelgen et al. reported a p-type MBT similar to the hybrid transistors mentioned in 2.2.4.2.2,but replacing also the inorganic semiconductor layer by NPB. This device contains NPB as emitter and collector layer [19], separated by a base of Ca/Al/Ca or coevaporated Ca/Al. Only after storage or heating in air for 5 min at 120 °C, the samples work reproducibly as transistors. As for the hybrid devices, it is assumed that the exposure to air leads to partial oxidation of the base electrode and opening of channels through the metal layer. For an operating voltage of 2.5 V, a current enhancement factor of 270 is calculated. As shown in fig. 2.14, the collector current (marked with squares) for zero base voltage is rather high.

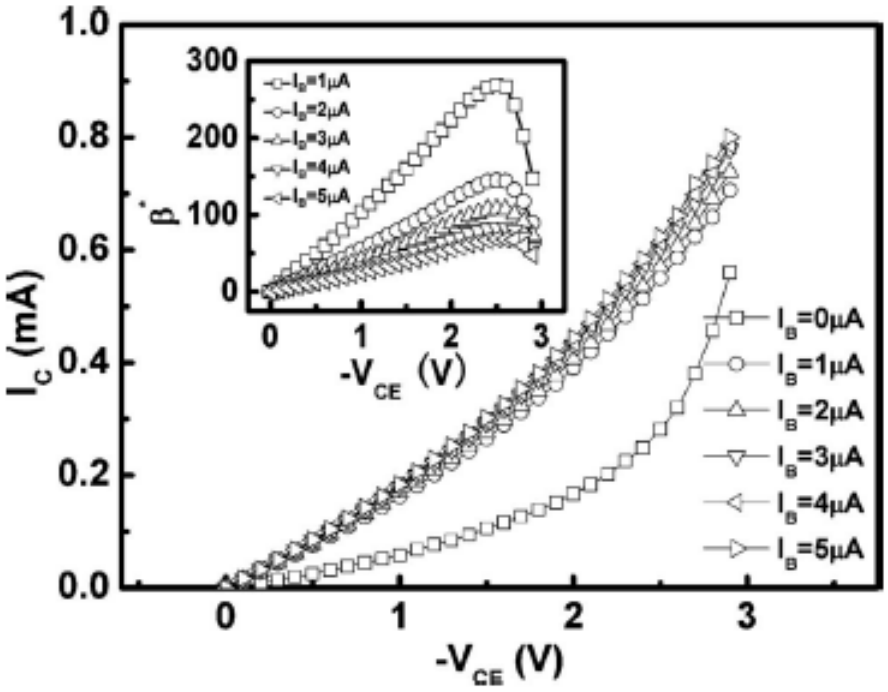

Figure 2.14: Output characteristics of a device containing a Al:Ca base electrode, taken from [19].

In the cases mentioned above, the formation of an inhomogenious base electrode incorporating pinholes is forced to obtain permeable base transistors. The workability of organic metal base transistors with a pinhole-free base electrode however was not proven until 2005 when Y. C. Chao et al. reported the "polymer hot-carrier transistor" [20]. The 9 nm thick Al base is evaporated on a spincoated layer of P3HT and results in a homogenous layer exhibiting a neglible roughness of approximately 2 nm. Thus, the authors propose a working mechanism based on hot carrier injection. As the mean free path within the base is supposed to be greater than the thickness, the probability of inelastic scattering is reduced and charge carriers are able to cross the electrode. The current enhancement factor of 25 is lower than the values of the organic PBTs mentioned so far, the collector current is found to be 0.5 mA cm^{-2} for operating voltages up to 5 V. An output characteristics is depicted in fig. 2.15.

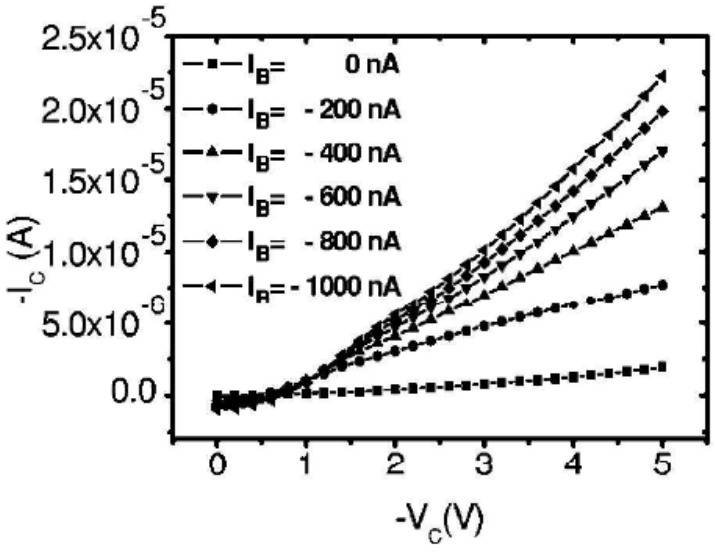

Figure 2.15: Output characteristics of a device containing a pinhole-free electrode, taken from [20].

While the working mechanism of the devices discussed so far can be sufficiently explained as either ballistic transport or transport through openings in the base electrode, Fujimoto, Nakayama et al. [2] reported in 2005 devices of similar structure which could not be undoubtedly identified as either permeable base transistor or hot-electron transistor. The devices are based on n-type organic semiconductors sandwiching a metal base electrode prepared by simple shadow evaporation. A collector layer of N,N'-dimethyl-3,4,9,10-perylene tetracarboxylic diimide (MePTCDI) is evaporated on an ITO electrode, followed by an aluminium base (20 nm), an emitter layer of Buckminsterfullerene C_{60} (100 nm) and a silver top electrode. High collector currents up to 350 mA cm^{-2} are measured for operating voltages up to 5 V, as depicted in fig. 2.16.

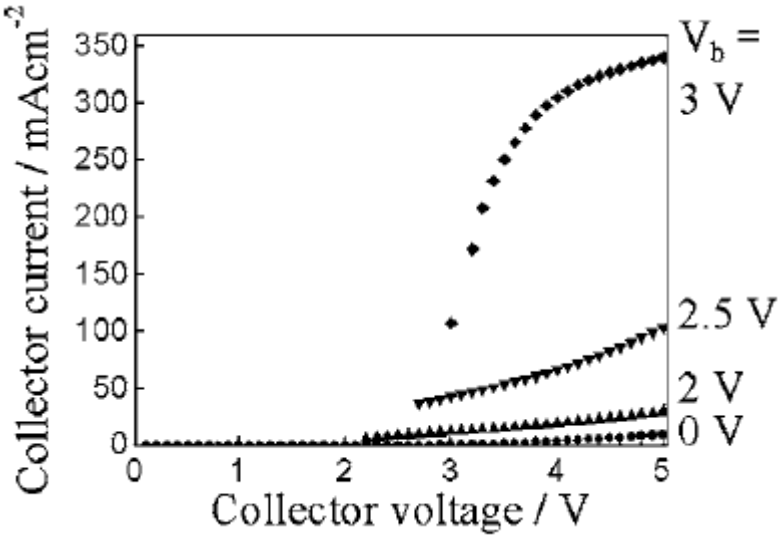

Figure 2.16: Output characteristics of a device containing a vacuum-evaporated base electrode between a MePTCDI collector layer and a C_{60} emitter layer, taken from [2].

The devices show an on/off ratio around several tens, which is greatly enhanced by air exposure after deposition of the base electrode as depicted in fig. 2.17 [21]. While the current enhancement factor reaches a maximum of 150, the on/off ratio increases to $3*10^5$ for operating voltages up to 7 V.

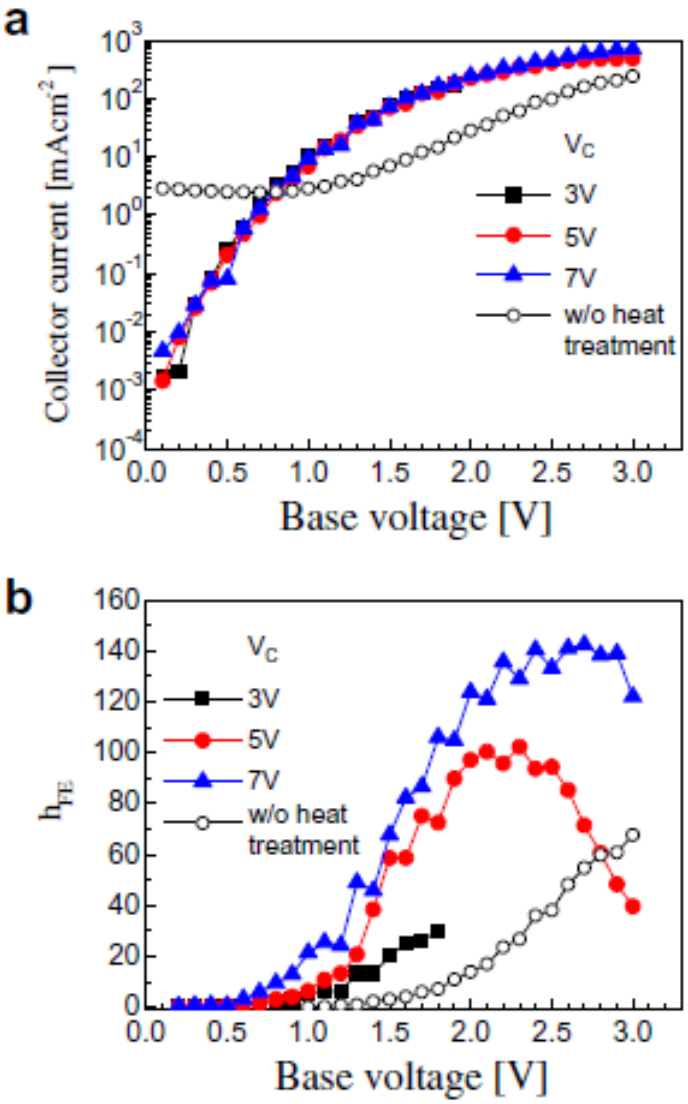

Figure 2.17: (a) Transfer characteristics, (b) current enhancement factor of a device subjected to a heat treament in air, taken from [21].

Many optimizations like the use of different emitter electrodes and additional layers have been reported [22, 23, 24]. The mechanism of electron transport through the base electrode is still unclear, both pinholes and ballistic transport are proposed as working principle.

The published transfer and output characteristics are measured in common-emitter mode. In contrast to the measurements on the hybrid transistors, the devices are measured fully voltage dependent, collector current and base current are recorded. When the current amplification factor is calculated, not only the leakage current $I_{c,off}$ but also the change in the base current throughout the

transfer measurement are taken into account by substracting the base current at zero base voltage $I_{b,off}$ from the actual base current I_b:

$$\beta = \frac{I_c - I_{c,off}}{I_b - I_{b,off}} = \frac{\Delta I_c}{\Delta I_b} \tag{2.10}$$

For the output characteristics, β is derived similarly for any collector voltage:

$$\beta = \frac{I_c - I_{c,off}}{I_b - I_{b,off}} \tag{2.11}$$

The graphs of collector and base current measured at zero base voltage are substracted from the corresponding graphs measured at a constant positive base voltage. Thus, the ratio of the changes in collector and base current is calculated, taking the major contribution of off current into account.

While in the VOTs mentioned so far, the charge carriers have to cross the current modulating electrode, Y. Yang et al. published a vertical organic field effect transistor (VOFET) of similar geometry, but different working principle [25]. On top of a capacitor cell with high charge-storage capabibility, an active cell is built, thus the following structure is achieved: gate - dielectrics - source - n-type organic semiconductor - drain, as depicted in fig 2.18.

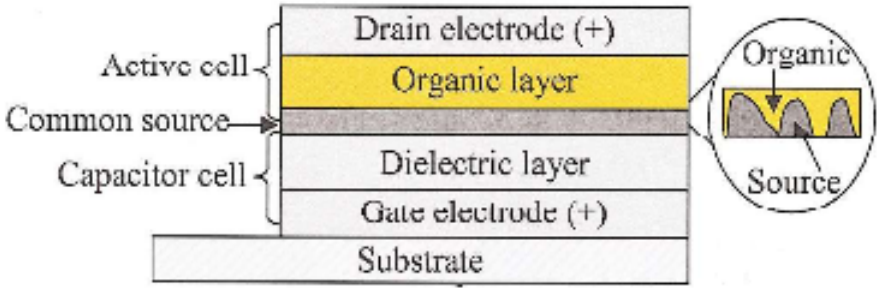

Figure 2.18: VOFET consisting of an active cell built on top of a capacitor cell with a thin a rough commn source electrode, taken from [25].

Due to a mismatch of the energy levels of semiconductor and source at zero gate voltage, low leakage current is observed. At positive gate voltage with repsect to the source, the capacitor cell is charged up and negative cahrge is built up within the very thin source electrode. Thus, a positive charge is built up in the semiconductor close to the source electrode, the effective energy barrier height for electron injection into the semiconductor is decreased. For a device incororating LiF as capacitor and C_{60} as semiconductor, an on/off ratio of $4*10^6$ and a high current output of 4 A cm^{-2} are measured. For solution-processed VOFETs incorporating poly(3-hexylthiophene) (P3HT), an on/off ratio of 10^3 and 0.4 A cm^{-2} are found by Y. Yang et al. [26]. The same group published the use of a light emitting polymer in the active cell in 2007, thus building a light emitting vertical

organic transistor [27].

Part II

Experimental

3 VOT preparation

3.1 Device geometry

The graphs shown in part III are all recorded from devices built in the following geometry:

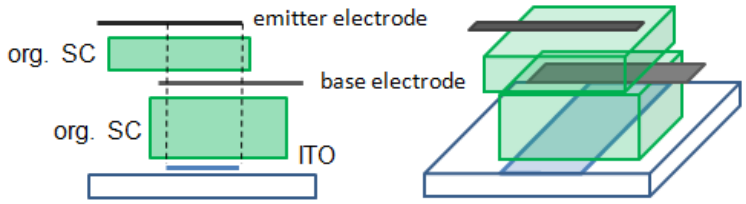

Figure 3.1: Device structure, only one of the two identical transistors built on one substrate is shown.

The nomenclature of the layer is similar to the wellknown inorganic bipolar transistor. The electron flux from the emitter (top) to the collector (bottom) electrode is modulated by the base (middle) electrode.

Glass squares sized 15*15 mm^2 serve as substrates, the indium tin oxide (ITO) stripe which is used as bottom electrode is depicted as light blue line or stripe in fig. 3.1. A thin aluminium base electrode is embedded between two layers of organic semiconductors, marked as green rectangles or boxes. The metal emitter electrode forms the topmost layer.

The ITO electrode on each substrate forms a 4 mm broad stripe from top to bottom in the middle of the glass. Two devices are built on one substrate, both using the same collector electrode. Shadow-masks with two parallel cut-out rectangles of 4*6.5 mm^2 are used for evaporation of the semiconductors, overlapping the ITO electrode one one side 0.75 mm, on the other one 2.5 mm. 2 mm broad base electrodes are evaporated perpendicularly to the collector electrode. For deposition of the second semiconductor layer, the same mask as for the first one is used just being turned upside-down, thus forming the broader overlap on the opposite side. When the 1 mm broad emitter electrode is deposited on top, it defines the active area of one device, which is the overlap of collector and emitter electrode, as 1*4 mm^2.

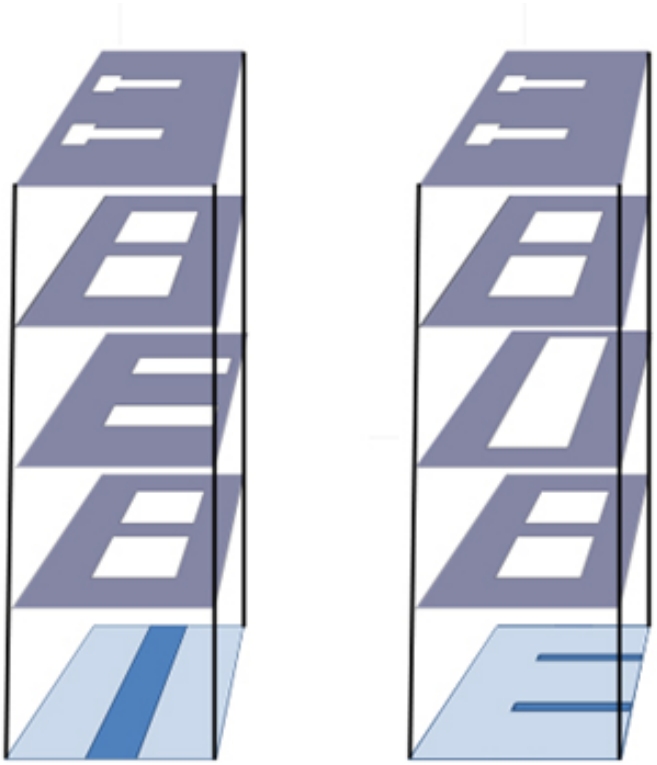

Figure 3.2: The left column (glass substrate with ITO electrode and masks in order of use) shows the mainly used geometry, the right column depicts the reference geometry with a bigger base area.

To exclude a working mechanism based on edge effects, a second geometry is used for a few samples, th mask geometry is shown in fig. 3.2 in the bottom row. Here, the base electrode is chosen in such a size that the semiconductors are separated completely whereas in the geometry described above, they touch each other at the edges of the Al. To be able to contact the ITO in this configuration, it is etched in the form of two 1 mm broad stripes, overlapping the parallel emitter electrodes on an area of 4 mm^2.

3.2 Substrate preparation and collector electrode ITO

The devices are built on top of glass substrates cut to squares of 15 * 15 mm^2 covered with indium tin oxide (ITO), purchased at Kintec, with a resistance of 15 Ω/sq. The ITO has to be removed partially, the remaining stripes serve as collector electrode. Insulating tape, which is cut to the requested geometry, is used to protect the electrode area during the etching process. The devices are etched for 15 min in a 4.6 : 0.4 : 5 mixture of hydrochloric acid : nitric acid : water, immersed in an ultrasonic bath (VWR Ultrasonic Cleaner) at room temperature. After the insulating tape stripes are removed from the rinsed samples, residues of glue are wiped off mechanically with cotton tips and acetone.

Afterwards, the samples are cleaned for 20 min each in acetone, methanol and isopropanol in the

ultrasonic bath and rinsed with 18 MΩ water before drying.

3.3 First semiconducting collector layer: MePTCDI

N,N'-dimethyl-3,4,9,10-perylene tetracarboxylic diimide (MePTCDI), which is used as collector layer for all devices, is a small molecule widely used as pigment, named Paliogen Red 179, because of its long term stability in air and deep red colour. The molecular structure is shown in fig. 3.3Due to its high absorption in the visible range from 400 to 600 nm, it was tested as well as a great variety of different perylene derivatives in the 1990s for solar cells [28, 29]. For the lowest unoccupied molecular orbital (LUMO) values ranging from 4.4 to 4.6 eV are reported, for the highest occupied molecular orbitals the published values range from 6.5 to 6.8 eV [24, 28]. As the energy levels were not measured during this work, mean values of the HOMO and LUMO levels of 4.5 and 6.7 eV, respectively, are assumed.

According to Graaf et al. , the electron mobility is found to be $5.6*10^{-4}$ cm^2 V^{-1} sec^{-1} at room temperature for an amorphous layer [30].

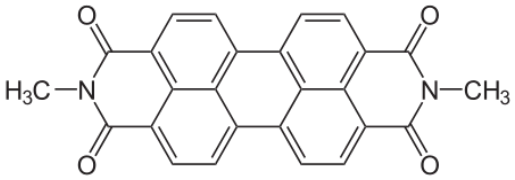

Figure 3.3: Molecular structure of MePTCDI

The MePTCDI used throughout the experiments is purchased from Hoechst AG and cleaned twice by resublimation at a pressure of 10^{-6} mbar. It is evaporated onto the substates in an Edwards high vacuum system (Manor Royal, Sussex) with a rate of 0.6 to 1.0 nm sec^{-1} at a vacuum better than $5*10^{-6}$ mbar. The average thickness of 500 nm varies within each batch up to 15 % because of inhomogenious evaporation over the area of the substrate holder. The samples are transferred to a glovebox (MBraun 150M-G) with nitrogen atmosphere immedeately after evaporation.

3.4 Base electrode: Al

Aluminium (Al) has a work function of ca. 4.3 eV which is slightly higher than the LUMO of MePTCDI, leading to a good electron injection contact [31]. The base electrode is deposited in a Leybold AS053 evaporation system at 10^{-6} mbar, using a tungsten boat and shadow-masks with a steel foil thickness of 200 μm.

Trying to optimize the device performance, different rates and ramps are chosen for evaporation, mainly a slowly increasing rate from 0.02 to 0.12 nm sec^{-1} and a constantly high rate of about 1 nm sec^{-1}.

3.5 Second semiconducting layer: C_{60} or MePTCDI

Buckminsterfullerene C_{60} is widely used as semiconductor in organic thin film transistors (OFETs) and solar cells [32]. The molecular structure is depicted in fig. 3.4. In 2002, the LUMO of PCBM was measured to be at 4.2 eV [33] by D. Mühlbacher. As the LUMO of C_{60} is widely known to be 0.1 eV lower than the one of PCBM, a value of 4.3 eV is assumed, with the according HOMO of 6.1 eV, a bandgap of 1.8 eV results. Depending on the measurement technique, however, LUMOs up to 3.8 eV are found in literature, leading to a bandgap of 2.5 eV [34].

The C_{60} used for the experiments is purchased at MER Corporation and has, due to sublimation, a purity of 99.9 %. Before use, it is resublimed in high vacuum to further reduce impurities.

To apply the semiconducting layer between base and emitter electrode, the samples are taken out of the glovebox and placed in the substrate holder in air. 100 nm of C_{60} are deposited in the evaporation system Univex 350 (Leybold) at high vacuum (10^{-6} mbar) at a rate of 0.16 nm sec^{-1}. After evaporation, the devices are again exposed to air when transferring them to the glovebox for deposition of the top electrode.

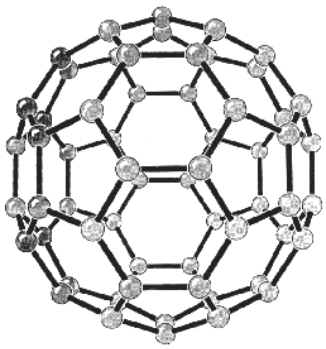

Figure 3.4: Molecular structure of buckminsterfullerene C_{60}

Apart from C_{60}, also MePTCDI is used for some devices as emitter layer. The evaporation of 100 nm MePTCDI is performed in the Edwards system as described in section 3.3 at a rate of 1 nm sec^{-1}.

3.6 Emitter electrode: Ag, Al and Cr

Silver (Ag) exhibits a work function of ca. 4.3 eV, depending on the structural orientation [31]. The evaporation of the top electrode is performed at high vacuum in the same system as the application of the base electrode (for details see 3.4). The deposition rate is chosen for all devices at 0.1 nm sec^{-1}, the layer thickness is 30 nm.

To investigate the effect of the emitter electrode material on the devices, different metals are used for the top electrode for the devices comprising MePTCDI as both emitter and collector semiconductor. Aluminium is deposited at a constant rate of 0.1 nm sec^{-1}. Chromium, which exhibits a work

function of 4.5 eV, is evaporated at a rate of 0.05 nm sec^{-1} [31].

3.7 Influence of heat treatment on the performance

As reported by K. Yutani et al., in the case of MePTCDI/C_{60} transistors improved results are achieved for devices which are heated after the base electrode deposition for two hours to 150 °C in air [23]. This leads to further decrease of the off current while the on current is only slightly effected, the on/off ratio reaches 10^5. As this improvement is not observed for devices subjected to a heat treatment under inert conditions, the authors attribute the positive effect to the formation of an oxide layer on top of the aluminium.

Based on these observations, the effect of heat treatment on the devices built for this work is tested. After Al evaporation, the samples are taken out of the glovebox and put on a heating plate set at 150 °C. The final layers are deposited after an annealing time of one or two hours.

4 Resistance measurements

4.1 Percolation

To find the thickness of percolation in a measurement, the following device is realized: A glass plate of 15*15 mm^2 is cleaned in an ultrasonic bath in a 3 : 1 mixture of ammonia (NH_4OH in water, 25 %) and hydrogen peroxide (H_2O_2 in water, 36 %) in water at 80 °C for 15 min, rinsed with water and dried. 500 nm MePTCDI are evaporated according to 3.3 without using a mask, thus covering the surface completely with the semiconductor. Two aluminium stripes with a thickness of 50 nm are deposited with a rate of 0.1 nm sec^{-1} in the metal evaporation system mentioned in 3.4. For this step, the mask which was previously used for the base electrodes is chosen because of the simple geometry, leaving a MePTCDI covered area of 3.5*8.75 mm^2 in between.

To connect the Al contacts to the measurement setup, the sample is exposed to air to braze one wire on each contact with Indium before the device is placed in the Leybold Univex evaporation system. The wires are connected to a Keithley 2400 to measure the resistance between the contacts during the evaporation of 30 nm Al on the sample (rate of 0.1 nm sec^{-1}). When percolation is reached, the two Al contacts are connected by the deposited Al layer, the resistance decreases rapidly.

4.2 Heat treatment

The oxidation of the base electrode, which is usually accelerated by heating of the sample [21, 16], is a crucial step for the preparation of reproducibly working transistors. This is confirmed in our own experiments with the data shown in 7. Therefore, the resistance measurement is carried on after finishing the percolation experiment. The evaporation chamber is flooded with air, the copper block serving as substrate holder is heated to 150 °C and kept at this temperature for 2 hours.

5 Measurement equipment

5.1 Electrical measurements

The electrical measurements are carried out under inert conditions (nitrogen) in a glovebox. As both C_{60} and MePTCDI are wellknown materials for organic solar cells, the samples are measured in the dark. All devices are measured in common-emitter mode, both base and collector are biased positively with respect to the grounded emitter. For the measurements, an Agilent Technologies system (E 5273A) is used. If not noted differently, hold time, delay time and step delay are set to 0.1 sec.

For each device, output and transfer characteristics are recorded. In the transfer characteristics, the collector current I_c is measured as function of the base voltage V_b at a constant collector voltage V_c. The on/off ratio and the current enhancement factor are calculated from the transfer characterstics. The collector current is measured in dependence of the collector voltage for different constant base voltages to obtain the output characteristics.

The current amplification factor is calculated like described in 2.2.4.3, base and collector current at Vb = 0 are taken into account according to literature [22].

5.2 Atomic force microscope

To investigate the surface mophology of the MePTCDI layer serving as a substrate for the base electrode deposition, a Nanoscope Dimension^{TM} 3100 atomic force microscope from Digital Instruments is used in tapping mode to avoid any damaging of the organic material.

5.3 Electron microscopy

The surface morphology of base electrodes with and without 1 h heat treatment is examined by scanning electron microscopy (SEM), additionally the cross sections of two full devices, again one with and one without 1 h heat treatment, are investigated. N-doped silicium wafers (phosphorous, 2-7 Ωcm^{-2}) serve as substrates. Four squares of 15*15 mm^2 are cut from the wafer, the oxide layer on top is etched with hydrofluoric acid. The ITO electrode is omitted, the organic collector layer (MePTCDI) and the base electrode (Al) are deposited directly on the silcium wafers as described in 3. Two devices are subjected to a 1 h heat treatment at 150 °C on the heating plate, two are not heated. One sample each is examined by SEM, using a ZEISS 1540 XB Cross Beam electron microscope and an InLens detector which is placed directly around the electron source, thus detecting secondary electrons.

Onto the two devices, which are not used for the SEM measurement of the base electrode, 100 nm MePTCDI layer and a silver top electrode are evaporated. The cross section of these complete samples is examined with the InLens detector.

Part III

Results and Discussion

6 Performance of VOTs based on MePTCDI and C_{60}

For this section, experiments of Fujimoto et al. are repeated and the resulting characteristics and parameters are compared to the reported ones [2]. The device preparation follows the guideline given in literature, for more information please see section 3. The energy diagram depicted in fig. 6.1 lists the work functions of the electrodes and the HOMOs and LUMOs of the semiconductors graphically (compare section 3).

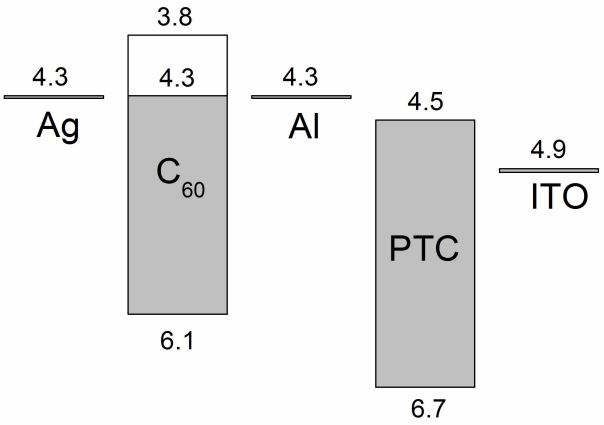

Figure 6.1: Energy diagram of a vertical organic transistor based on MePTCDI and C_{60}. As different values for the LUMO of C_{60} are found in literature, this is taken into account in the figure.

The output characteristics depicted in fig. 6.2 shows transistor behaviour, as the collector current for an applied base voltage exceeds the collector current which is obtained for zero base voltage (off current). The off current increases significantly with increasing collector voltage, reaching 50 mA cm^{-2} for 4 V collector voltage. When considering the base current recorded at this measurement, the graph displays a negative current like the collector current mirrored at the x-axis; an equivalent current of -50 mA cm^{-2} is found at 4 V collector voltage. Thus, an electron flux from base electrode to collector electrode like depicted as dotted line in fig. 6.3 can be assumed as off current.

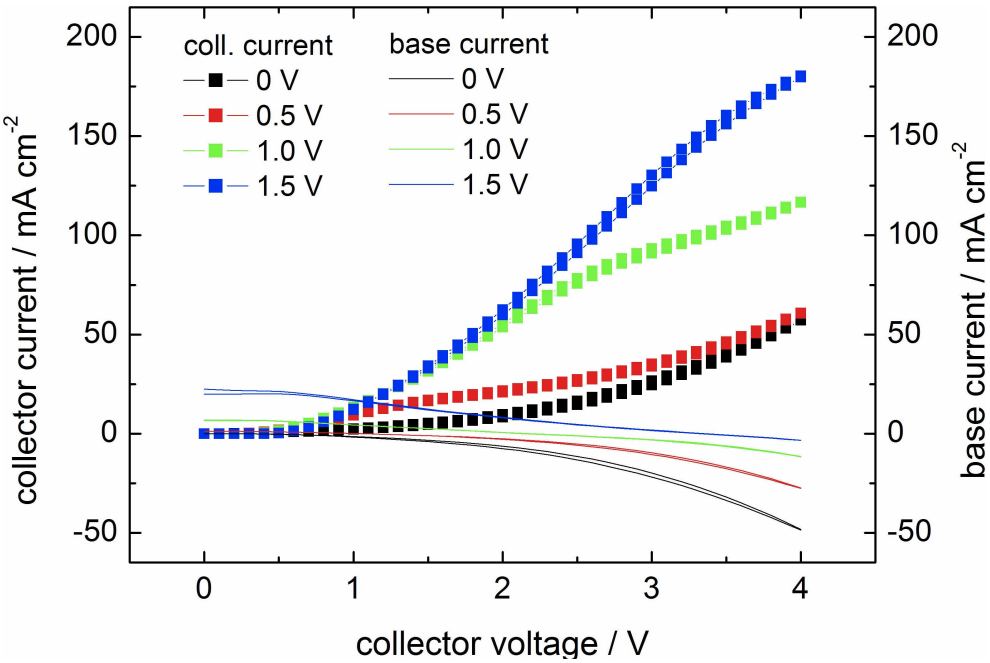

Figure 6.2: Output characteristics of a MePTCDI/C_{60}device without heat treatment. Collector current (lines marked by symbols) and base current (solid lines) are measured at different constant base voltages from 0 to 1.5 V.

Application of 1.5 V base voltage increases the collector current from 50 to 180 mA cm^{-2} at 4 V collector voltage, higher base voltage does not result in higher output current, saturation is reached. Output characteristics reported in [2] show saturation at higher voltages, at 3 V base voltage, more than 300 mA cm^{-2} collector current are measured.

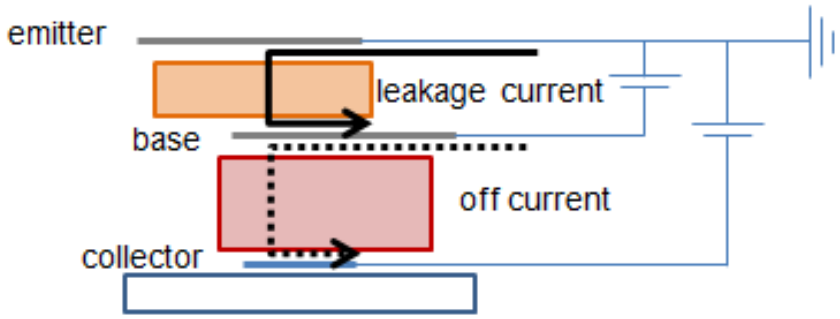

Figure 6.3: Off current and leakage current from collector to base electrode

High off current is again observed in the transfer characteristics shown in fig. 6.4, leading to an on/off ratio of 6 for a constant collector voltage of 3 V and an on voltage of 1.5 V. The large change in base current from -20 to +3 mA cm^{-2} results in a current amplification factor β of 5. This change of sign in base current shows a reversal of the electron flux in the base electrode. The base electrode acts as electron emitter for high collector voltage and low base voltage as described above for the off current (zero base voltage). Electrons are drawn from the base to the collector electrode due to the high electric field between collector and base. At higher base voltage, however, the base

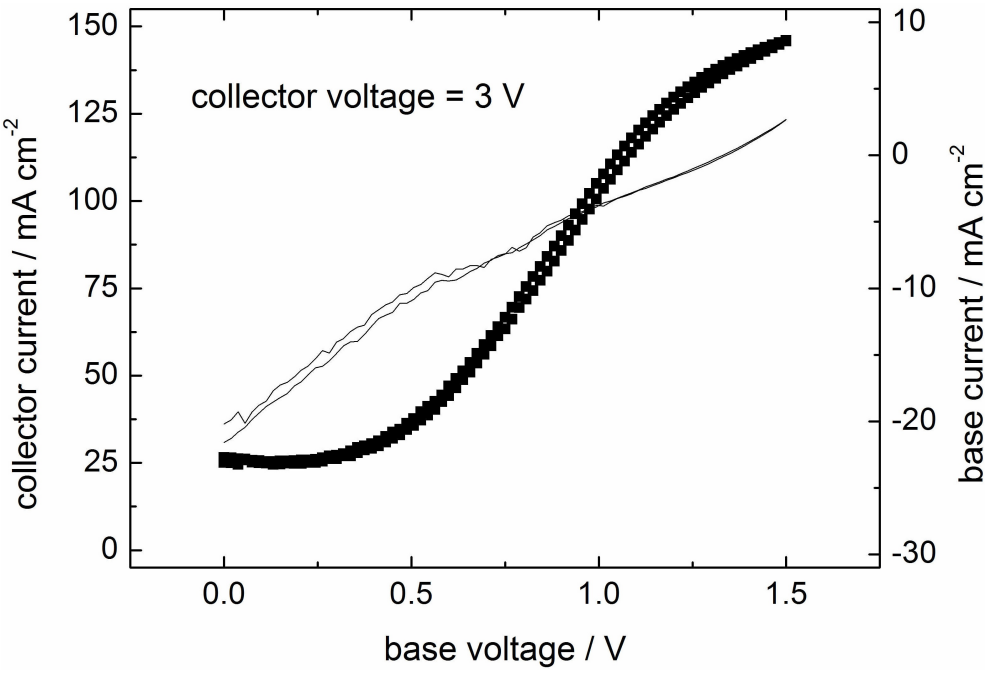

Figure 6.4: Transfer characteristics at $V_b = 3$ V of a MePTCDI/C_{60}device without heat treatment. The graph marked by squares represents the collector current, the solid line the base current.

electrode draws electrons from the emitter electrode because the electric field between collector and base lowered while a field between emitter and base is built up. The latter case is sketched in fig. 6.3 as black arrow and abbreviated as leakage current because the current flowing through the base electrode does not contribute to the output current and gives rise to a base transmission factor smaller than unity.

Similar performance is observed for the devices built in the second geometry described in 3.7. In this case, the semiconductors are completely separated by the base electrode to exclude the influence of edge effects on the measurement and the working mechanism. For both geometries, however, workable devices were only obtained in case of a slow base electrode deposition.

Although the devices show a transistor behaviour, the performance reached throughout the experiments is worse than reported elsewhere because of high off current and base current. A high percentage of the produced devices does not display any transistor behaviour. Additionally, bad reproducibility between the produced batches and within each batch is observed.

7 Effect of heat treatment

Annealing processes in air or inert conditions (vacuum, nitrogen) and with or without applied voltage are widely used in organic electronics to yield better performance and optimize characteristic device parameters [35]. It is known that they exhibit great impact on the surface morphology, recrystallisation and phase separation of organic materials and their blends [36]. Additional processes

can take place during the heating of an organic layer after deposition of a metal layer. Apart from interactions between the layers, such as diffusion processes of the metal into the organic material, also the effect of heating on the metal itself has to be taken into account [37]. Depending on its electron affinity, oxidation processes may play a role [16].

In case of vertical organic transistors, an oxidation/annealing step of the base electrode in air is found to clearly enhance the performance. For the devices containing NBP and a base layer consisting of Ca/Al/Ca mentioned in section 2.2.4.3, it is reported by J. P. M. Serbena et al. that transistor characteristics can only be observed when the devices are kept in air for some longer period of time after the deposition of the base electrode [16]. The same characteristics are observed for the devices after an exposure to air for only five minutes at a temperature of 120 °C, which should lead to faster oxidation. It is assumed that the Ca is oxidized completely, leading to pinholes in the base electrode.

Similar observations are made by K. Yutani et al. [23]. In the case of MePTCDI/C_{60} transistors, exposure to air leads to a lower off current and thereby to an improvement of the on/off ratio from approximately 40 to more than 300. Even better results are achieved by this group when the devices are heated after the base electrode deposition for two hours to 150 °C in air, which leads to further decrease of the off current. As the on current is only slightly effected, the on/off ratio reaches 10^5. When the device is subjected to the heat treatment before deposition of the base electrode, no effect on the performance is observed. This confirms the presumption that the exposure to air at elevated or room temperature has great impact on the metal or the metal-semiconductor interface. Additionally, heat treatment after evaporation of the base electrode in inert atmosphere is tested on some devices. Again, the performance does not improve significantly. Therefore, the positive effect of the heat treatment is attributed to partial oxidation of the base electrode [21].

To prove the positive effect of heat treament on the performance, devices are exposed for 1 h and 2 h to air at 150 °C. The resulting characteristics are depicted in fig. 7.1, fig. 7.2 and fig. 7.3. For all figures, the graphs in the left belong to a device heated for 1 h, graphs in the right to a device heated 2 h.

Comparing the output characteristics of the device without heat treatment to the one of the device with 1 h heat treatment, a decrease in the collector current at 3 V collector voltage and 1.5 V base voltage from 150 to 9 mA cm^{-2} is observed. Yet, the transfer characteristics show a even more pronounced decrease of off current and base current, leading to a significant improvement of the device parameters. An on/off ratio of 700 is observed for a collector voltage of 4 V and a base voltage of 1.5 V. β , which is calculated from the same transfer characteristics, reaches a maximum of 40 at 1.2 V base voltage.

A 2 h heat treatment further decreases the collector current, an on/off ratio of 200 is obtained. In the transfer characteristics, a significant increase of base current is observed for application of base voltage, the electron transfer ratio from emitter to collector is small, resulting in a maximum

β of 2. For a base voltage smaller than 0.75 V, the graph exhibits an artifact due to arithmetic reasons. For base voltage higher than 1.2 V, β decreases below 1, which means that the change of base current is greater than the change of collector current. Additionally, hysteresis of base and collector current is observed. This phenomenon is observed for most devices built for this work and is therefore discussed in a separate section (see section 10).

Reproducibility from batch to batch and within on batch increases slightly when comparing heated and not heated devices, but still only a small percentage of the built samples works sufficiently as a transistor.

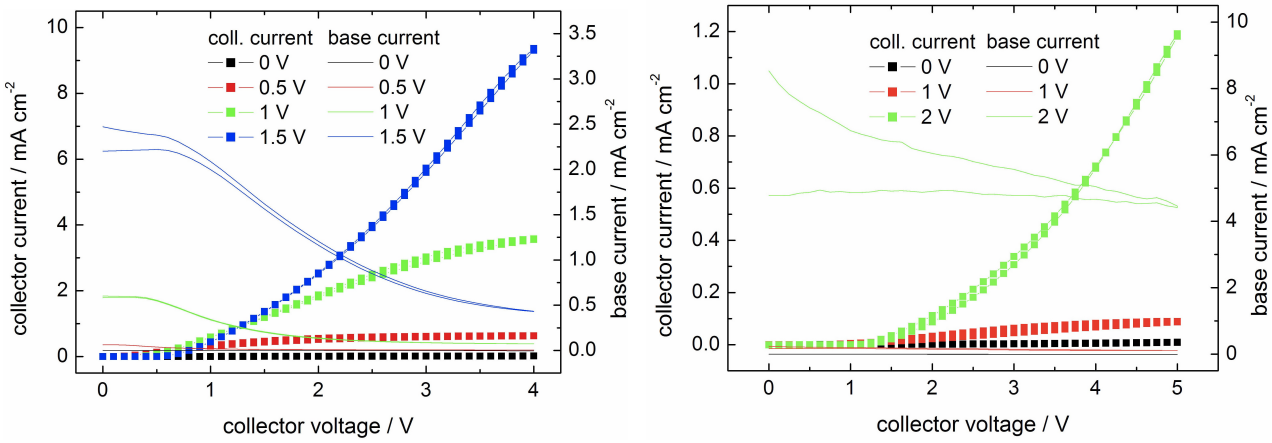

(a) 1 h heat treatment (b) 2 h heat treatment

Figure 7.1: Influence of different heating times on the performance. Output characteristics shown in the left figure were taken after 1 h of heating time, output characteristics in the right figure after 2 h heating time.

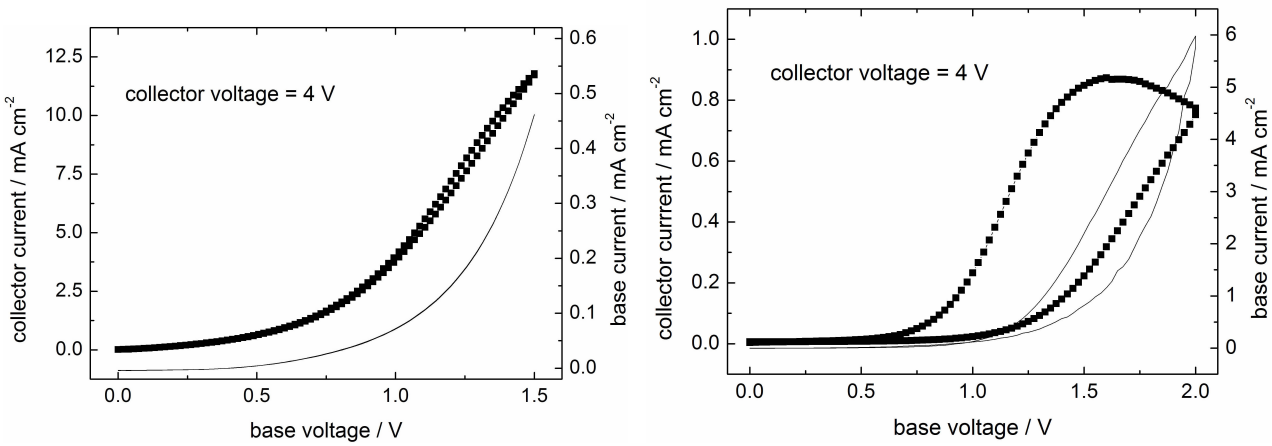

(a) 1 h heat treatment (b) 2 h heat treatment

Figure 7.2: Influence of different heating times on the transfer characteristics. The measurement shown on the left was taken after 1 h of heating time, the analogon on the right after 2 h heating time.

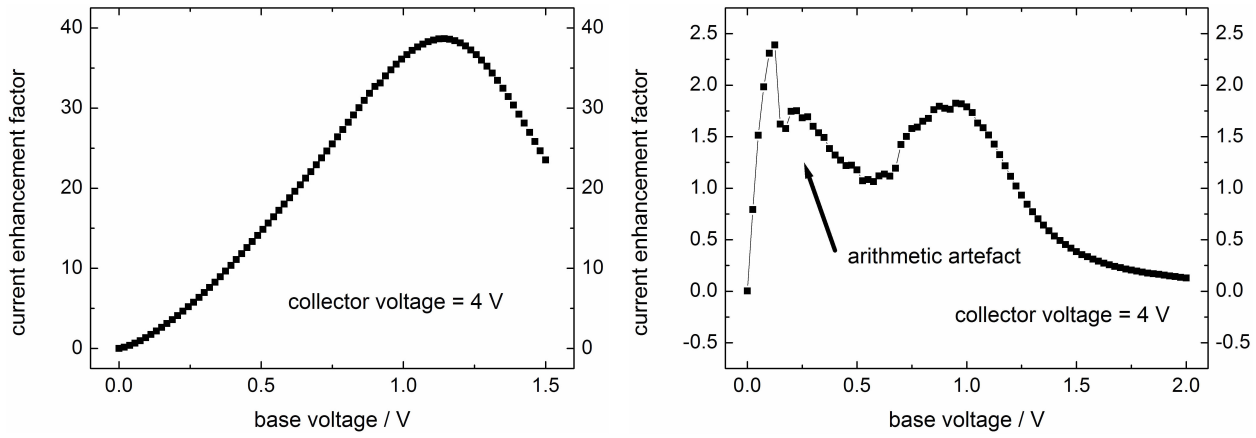

(a) 1 h heat treatment (b) 2 h heat treatment

Figure 7.3: Influence of different heating times on the current enhancement factor versus base voltage. The graph shown in the left figure was taken after 1 h of heating time, the analogon in the right figure after 2 h heating time.

Based on the results of this experiment, all transistor characteristics shown in the following chapters are obtained from devices subjected to a 1 h heat treatment at 150 °C.

8 Influence of the emitter electrode material

The working mechanism of the vertical transistors based on MePTCDI and C_{60} is still not fully understood, and when attempts have been made by Fujimoto and al. to change the semiconducting materials, no comparable transistor characteristics could be observed [2]. This indicates that apart from matching energy levels and a thin enough base electrode, additional properties of the components have great impact on the workability of the devices. While in section 11 attention is turned to the morphology of the base electrode and the underlying collector layer, this chapter deals with the effect of the emitter semiconductor and metal layer. MePTCDI is used instead of C_{60} as semiconducting layer between base and emitter electrode to exclude any influence of the change in energy levels between the semiconducting layers. Comprising the same material between the three electrodes, the structure resembles a triode in solid state, replacing vacuum with semiconductor and the geometrically well defined grid elctrode with an evaporated metal layer.

To investigate the electron injection at the emitter electrode, several metals exhibiting different work functions are used for the top contact. The semiconducting emitter material is changed to MePTCDI, thus parameters such as charge carrier mobility, crystallinity etc. stay constant throughout the semiconducting layers and their influence on the performance of the devices is minimized. Still, the comparison of devices containing different emitter electrodes is complicated by the significant variations of off current and base current within one batch of identically produced samples (for further information, see section 9).

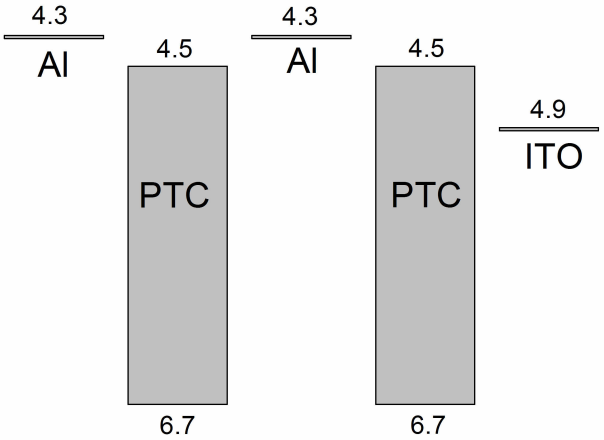

Figure 8.1: Energy levels of a device based on MePTCDI as emitter and collector semiconductor and Al as base and emitter electrode.

When using Al as emitter and base electrode for devices containing only MePTCDI as semiconductor, the following structure is obtained: ITO-MePTCDI-Al-MePTCDI-Al. The work functions of Al (4.3 eV) and Ag (4.3 eV) are of similar height, the slight difference may not affect the performance. Yet, it has to be taken into account that the oxidation process may change the work function of the base electrode. Fig. 8.1 shows a schematic grouping of the energy levels without taking the oxide layer into account.

The device characteristics depicted in fig. 8.2 show a fully working device. Although the device was subjected to a 1 h heat treatment, a high off current of 3.5 mA is observed in the transfer characteristics measured at 3 V collector voltage. An on/off ratio of 12 can be obtained for 2 V base voltage. The current enhancement factor β reaches a maximum of 14 at 1.75 V.

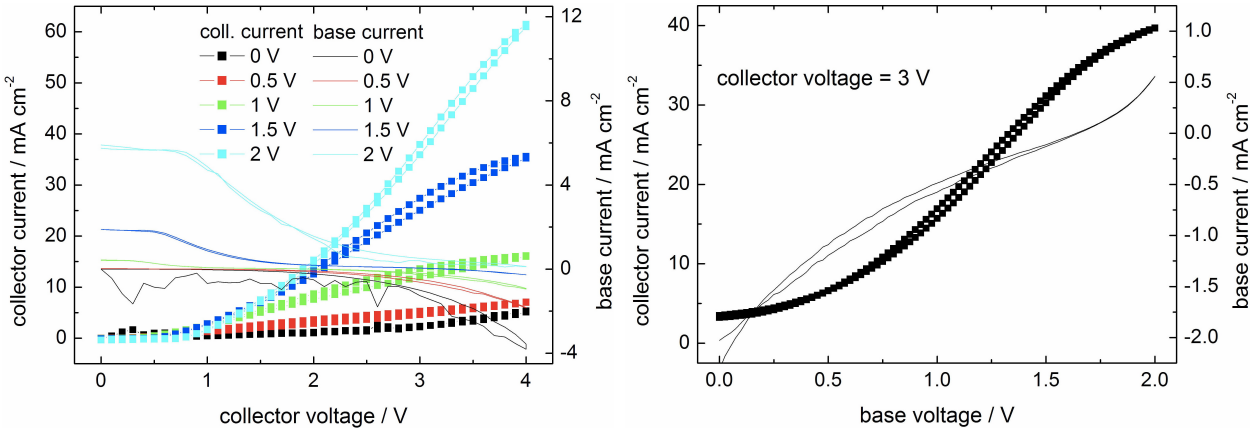

Figure 8.2: Output and transfer characteristics of a device comprising Al as base and emitter electrode and MePTCDI as emitter and collector layer.

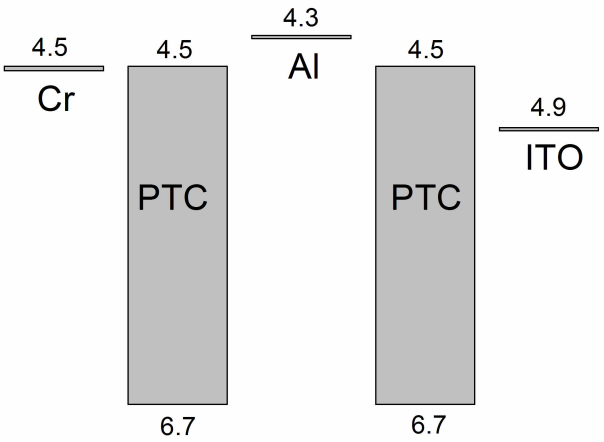

Figure 8.3: Energy levels of a device based on MePTCDI as emitter and collector semiconductor, Al as base electrode and Cr as emitter electrode.

As shown in the output characteristics, application of 2 V base voltage leads to an increase of the collector curent from 5 to 60 mA cm^{-2} for 4 V collector voltage. Compared to the devices comprising C_{60} as emitter which were subjected to a 1 h heat treatment, the devices discussed in this section show higher currents. The disproportionately higher base current and off current result in poorer device parameters.

Cromium (Cr) exhibits a work function of 4.5 eV, significantly lower than the work functions of Al and Ag, and close to the LUMO of MePTCDI (4.4 - 4.6 eV). Fig. 8.3 shows that electron injection works from Cr to MePTCDI if one assumes a HOMO level for MePTCDI lower than 4.5 eV.

Compared to the samples incorporating an Al emitter, the base current is significantly higher. As shown in the output characteristics in fig. 8.4, the collector current exceeds the base current only for a collector voltage higher than 3 V. The high base current affects the current enhancement factor negatively, a maximum of 4 is found.

Yet, the on/off ratio is better than with an Al top electrode, reaching 120 for a collector voltage of 5 V and a base voltage of 2 V.

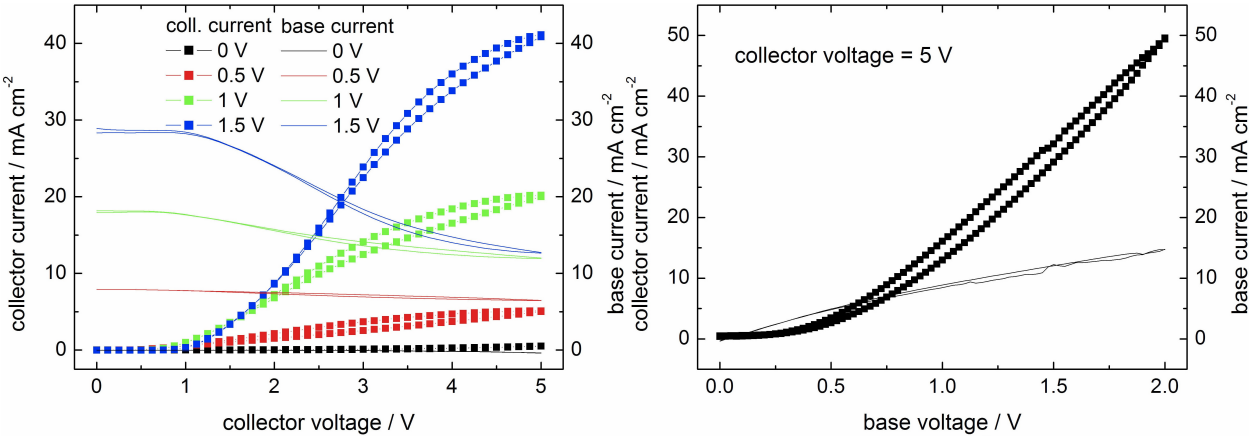

Figure 8.4: Output and transfer characteristics of a device comprising a cromium emitter and MePTCDI both as emitter and collector semiconductor show.

When using Ag as emitter electrode, the following characteristics (fig. 8.5) are obtained. For a collector voltage of 3 V and a base voltage of 1.5 V, a collector current of 35 mA cm^{-2} is found in the output measurement. The transfer chracteristics show a collector current of 75 mA cm^{-2} and a base current of only 0.6 mA cm^{-2} for a base voltage of 1.5 V and a collector voltage of 4 V.

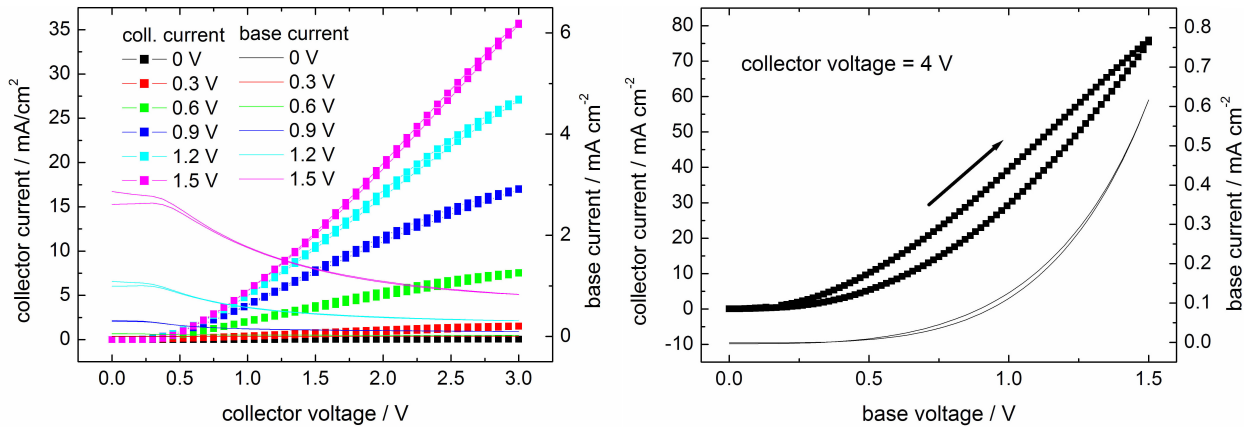

Figure 8.5: Output and transfer characteristics of a device comprising a silver emitter and MePTCDI both as emitter and collector semiconductor show.

Compared to the devices comprising Al and Cr emitters, by far the highest on/off ratio and current enhancement factor are obtained for the sample with an Ag emitter, at 500 and $2*10^3$, respectively. Additionally, the devices containing the silver top electrode work sufficiently as transistors at significantly lower input voltages. While similar values for the collector current are found for samples with Ag and Al emitters, the base current is clearly increased for the Cr sample. Comparing the collector current at 3 V collector voltage and 3 V base voltage in the output characteristics shown above, for all three devices values around 30 mA cm^{-2} are found while the base currents differ significantly.

9 Influence of the evaporation geometry

As mentioned before in section 8, the comparison of devices containing different materials is complicated by the significant variation in the performance of the devices built within one batch. Thus, in this section, possible explanations for these variations are discussed.

Two devices, which exhibit considerable differences in performance although they were produced in one batch, are shown in fig. 9.2. In the production, each step is done identically and at the same time for both samples, still base current and off current vary significantly. To simplify the comparison, the devices will be abbreviated with "device 1" and "device 2" for further discussion. The output characteristics plotted in the left were obtained from device 1, the output characteristics in the right from device 2.

As the devices are subjected to the same evaporations, the purity of the used materials and the evaporation conditions (vacuum, deposition rate, temperature, humidity at air exposure etc) are the same. The only observed difference is the position of the substrates on the sample holder during the evaporations. For both organic evaporations in the Edwards evaporation system, the two devices are put in close vicinity, the substrate edges are separated by just 2 mm. Within this distance it seems unlikely that thickness and roughness would vary enough to affect the performance significantly. For base evaporation, device 1 is placed directly above the boat while device 2 is placed on the far edge of the substrate holder. The evaporation angle of device 2 differs significantly from the 90 ° used for device 1. This is supposed to lead to shadow effects when evaporating a layer of 25 nm on a rough surface, an even more inhomogenious thickness of Al might be achieved. The same configuration of samples on the substrate holder is chosen for the Ag emitter electrode evaporation, but the holder is placed with its center exactly above the boat. Fig. 9.1 shows that distance and angle of evaporation should be nearly equal for both devices.

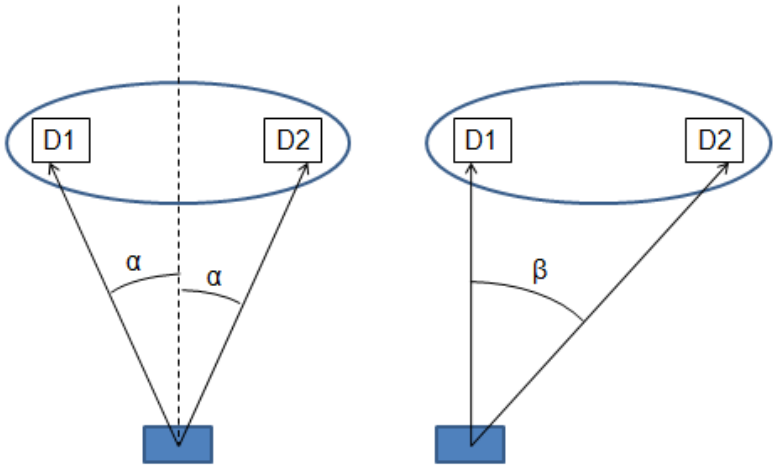

Figure 9.1: An exaggerated sketch of the evaporation angles for deposition of the emitter electrode on the devices 1 and 2 (abbreviated with D1 and D2) is shown in the left picture; the box at the bottom marks the boat. For the deposition of the base electrode, the substrate holder is shifted, a situation as depicted in the sketch on the right is obtained.

While device 1 and 2 show similar collector currents in the transfer and output chracteristics in fig. 9.2, device 1 exihibits a significantly higher base current of 15 mA cm^{-2} maximum in comparison to 3 mA cm^{-2} for device 2 measured at zero collector voltage for 1.5 V base voltage in the output characteristics. The on current for 3 V collector voltage is found to be around 35 mA cm^{-2} in both cases.

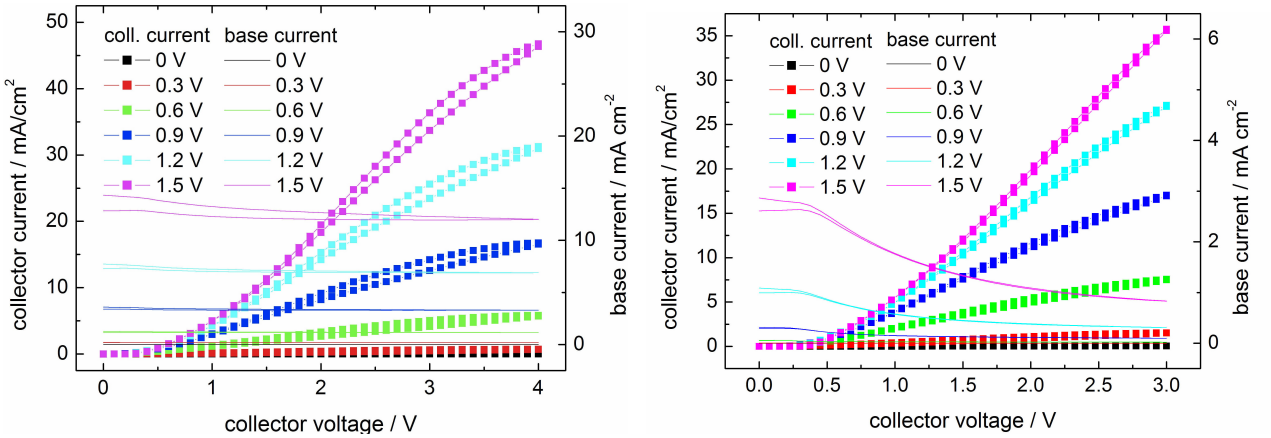

(a) Device 1 (b) Device 2

Figure 9.2: Two devices out of the same batch are compared, output characteristics of device 1 are shown in the left figure, output characteristics characteristics of device 2 in the right figure.

The high base current of device 1 is also observed in the transfer characteristics in fig. 9.3 and is responsible for the maximum β of 8, while device 2 exihibits values up to 500 around 0.4 V base voltage for the same collector voltage of 4 V, as shown in fig. 9.4. In the same measurement, the on current is in both cases found to be 80 mA cm^{-2} while the off current for device 1 is almost a factor 5 lower than for device 2. Thus, the on/off ratio varies within one batch from 10^4 to $2*10^3$.

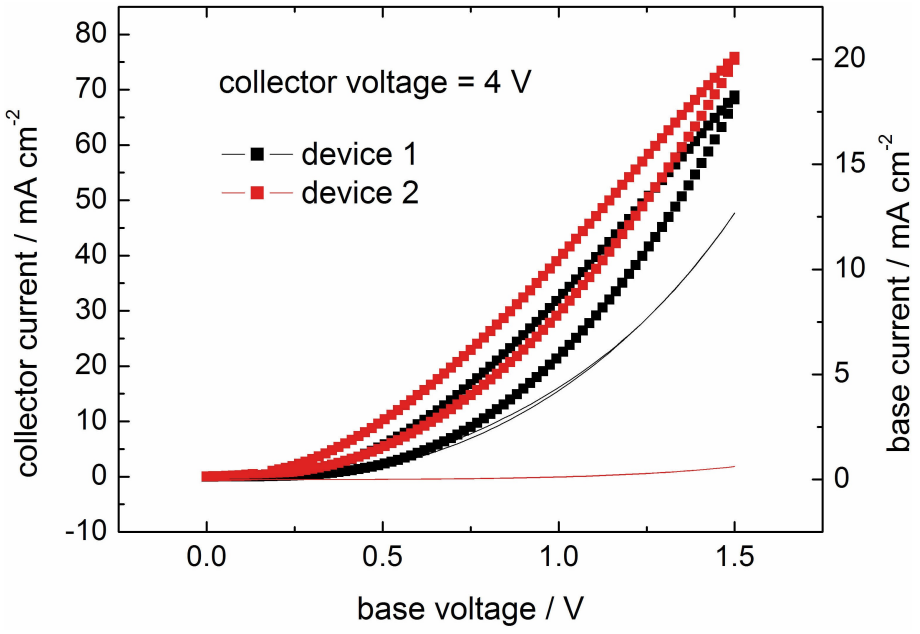

Figure 9.3: Transfer characteristics of device 1 (black) and device 2 (red).

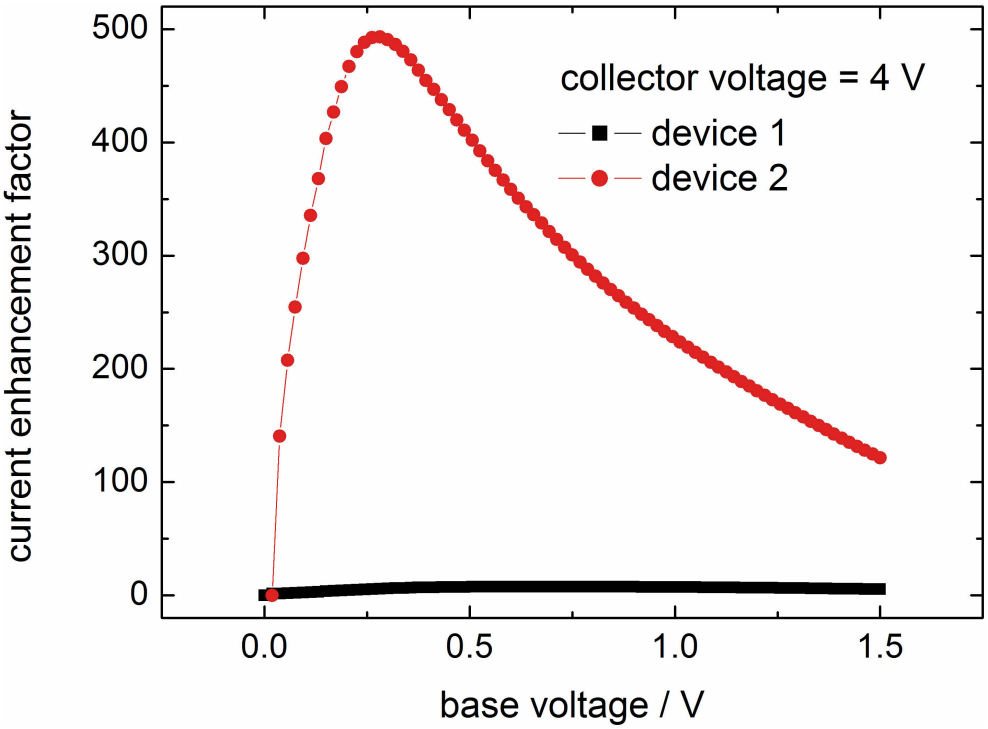

Figure 9.4: Current enhancement factor versus base voltage for device 1 (black) and device 2 (red).

10 Hysteresis

For both devices shown in section 9, a hysteresis exhibiting a lower backsweep current is observed. This may indicate that a barrier for the electron transport is built up during the forward sweep which lowers the backsweep current. Hysteresis has been observed and investigated in case of organic field effect transistors, different mechanisms have been proposed for higher and lower backsweep current hysteresis. Trapping of majority carriers at an semiconductor / dielectric interface and impurities of the organic layer may cause a lower backsweep current and can be influenced by oxygen, water and OH groups of the dielectric acting as electron traps. [38]

The organic vertical transistor does not incorporate a dielectric layer as such, therefore the knowledge gained from investigations on the interfaces of OFETs cannot be applied directly. Yet, in case of a heat treatment in air of the Al base electrode, the growth of an aluminium oxide layer on top of the electrode is assumed. Due to passivation of the surface, the thickness of this layer is expected to be in the range of Angströms up to nm, while for OFETs an oxide thickness in the range of several tens of nm is grown by electrochemical anodization [39].

At the interface of this insulating alox layer and the MePTCDI evaporated on top, electrons may be accumulated at the application of a positive base voltage: Alox acts as capacitor. When the base voltage is decreased again, the shielding effect of the accumulated negative charge counteracts the applied positive base bias and leads to a lower backsweep current observed in the graphs.

Device 2 is additionally measured using different time scales to gain information on the time scale of the hysteresis, the resulting graphs are shown in fig. 10.1.

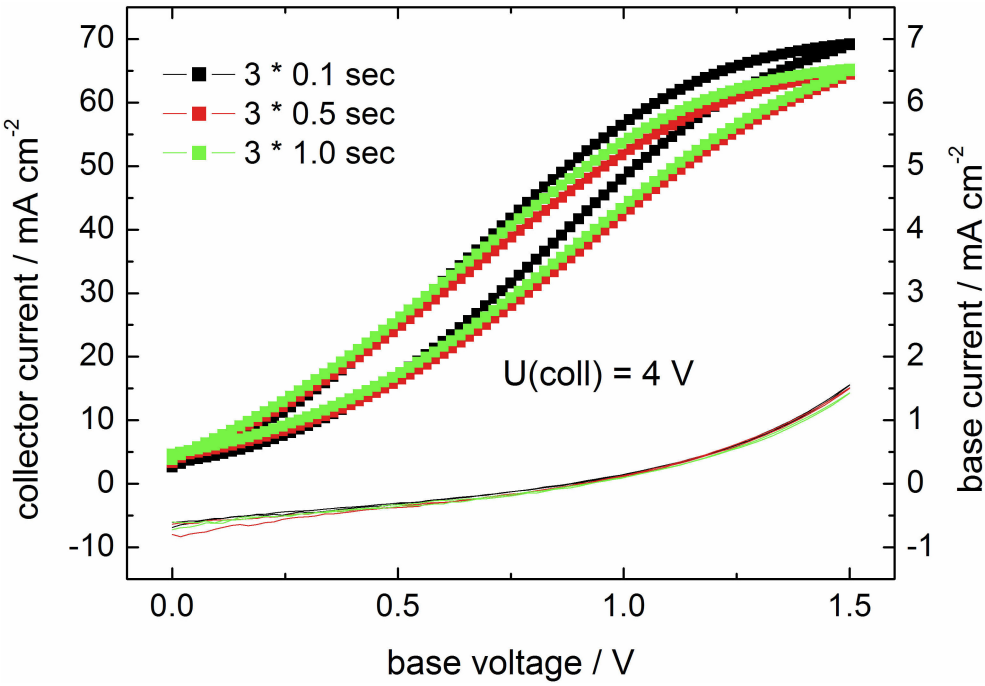

Figure 10.1: Device measured with different time scale, similar hysteresis is observed.

For time scales in the order of 0.1 to 1 sec, the width of the hysteresis stays constant, the maximum collector current decreases slightly for time scales higher than 0.1 sec.

Publications on vertical organic transistors do not deal with the subject of hysteresis in the various architectures yet. The graphs depicted in section 2.2.4.2.2 and 2.2.4.3 do not show full measurement circles from minimum to maximum and back to minimum voltage, but only a one-directional sweep. Without the backsweep, no hysteresis can be observed and compared to the hysteresis found during this work.

However, a similar structured device was inestigated by Y. Yang et al. in 2006 [40], both the device structure and the hysteresis graph are depicted in fig. 10.2. The hysteresis effect in these bistable organic devices is attributed to the formation of Al nanoclusters in the middle electrode, which is enhanced by coevaporation of 2-amino- 4,5-imidazoledicarbonitrile. Further analysis of the nanoclusters shows an aluminium oxide shell around each ca. 25 nm cluster which is supposed to be formed by reaction with oxygen or 2-amino- 4,5-imidazoledicarbonitrile [41]. As shown in section 11, the base electrode of the devices produced for this thesis is formed of crystallites in the size of 100 nm, the heat treatment in air is supposed to lead to surface oxidation. Thus, certain similarities to the published devices can be found, however, detailed investigation of response times etc. have to be done to allow further comparison.

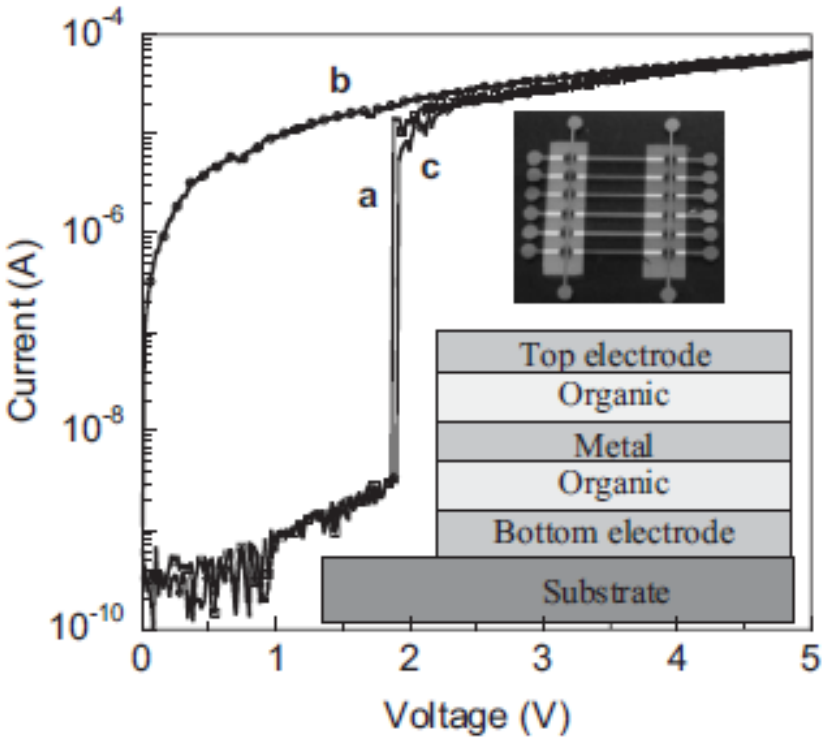

Figure 10.2: Device structure and measured hysteresis in an organic bistable device, taken from [40].

11 Morphology of the base electrode

In 2005, the first organic vertical transistors based on MePTCDI and C_{60} were published [2]. In this paper, a study on the effect of the base thickness on the base transmission factor and the current amplification factor is presented. The base transmission factor approaches unity for a thickness up to 40 nm, for thicker layers a significantly increased base current is measured, resulting in poorer transmission and a current enhancement factor β decreasing to values lower than unity. Similar observations are made by Cheng et al. when varying the Al base thickness in vertical organic transistors incorporating copper phthalocyanine as semiconductor [42].

While many optimizations of the base electrode, e.g. coevaporated alloys, multilayered electrodes, network-like structures and exposure to air, have been reported, the influence of the morphology of the underlying layer and the base itself is not yet investigated in detail. AFM pictures published for the vertical organic transistors mentioned before show the surface of the semiconductor layer serving as substrate for the base evaporation. Although different materials (CuPc and MePTCDI) are used, both pictures show grain-like crystals with a diameter of around 100 nm and a surface roughness in the range of 70 nm. AFM pictures of the devices prepared for this work are taken for comparison.

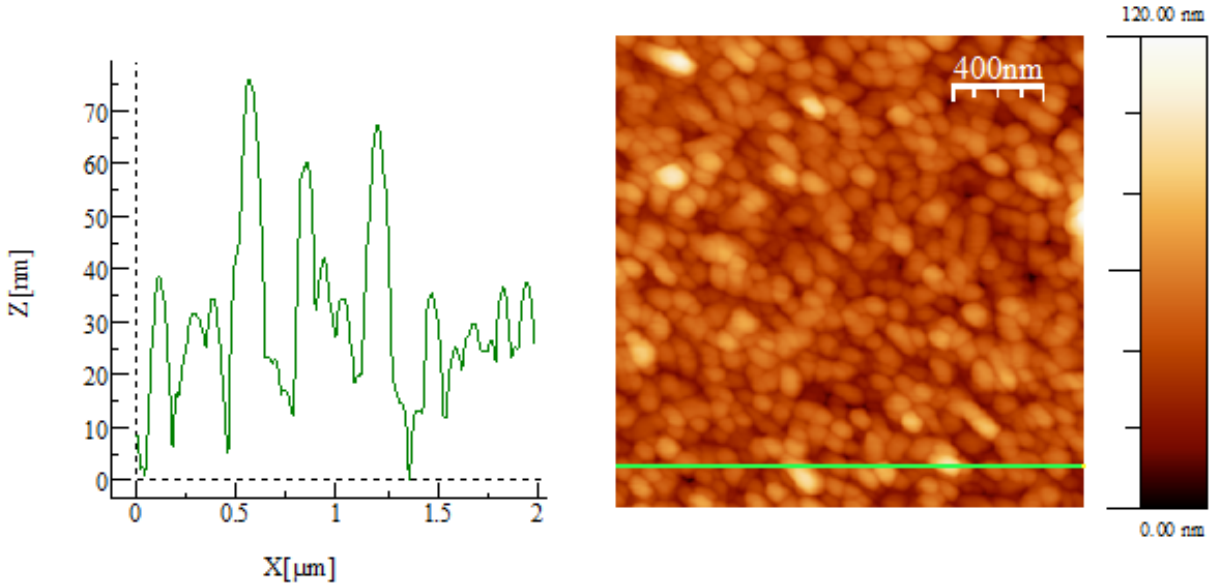

Figure 11.1: The AFM picture of a MePTCDI layer deposited at high rate shows grain-like crystals of 100 nm and a roughness of 70 nm.

Fig. 11.1 shows a 2*2 µm picture and a height profile of a 500 nm MePTCDI layer evaporated at a high deposition rate of 1 nm sec^{-1}. Both grain size and surface roughness are found to be in the same range as the reported values. When evaporating a 25 nm layer of Al on this surface, the formation of a unique nanomorphology can be assumed. The high roughness in comparison to the thin Al base on top may give rise to an inhomogenious layer thickness, shadow effects and a very high metal surface area.

To obtain further information on the morphology of the base electrode, it is investigated by scanning electron microscopy (SEM). As the scanning of the MePTCDI layer with an electron beam leads to immedeate accumulation of charges, the MePTCDI layer cannot be examined directly. To allow this measurement, the organic surface would have to be sputtered with a metal. As the resulting structure (MePTCDI with thin layer of metal) would resemble the base electrode, the metal base electrode is measured directly. Fig. 11.2 shows images of the Al base electrode. Pictures of a device subjected to a 1 h heat treatment are shown beneath the images of a not annealed sample, but no obvious difference be observed. While the crystallites of MePTCDI were interpreted as grains in the AFM, the SEM reveils crystallites formed like curved needles protuding in different angles from the surface, growing threedimensionally around each other and leaving holes and cavities in between.

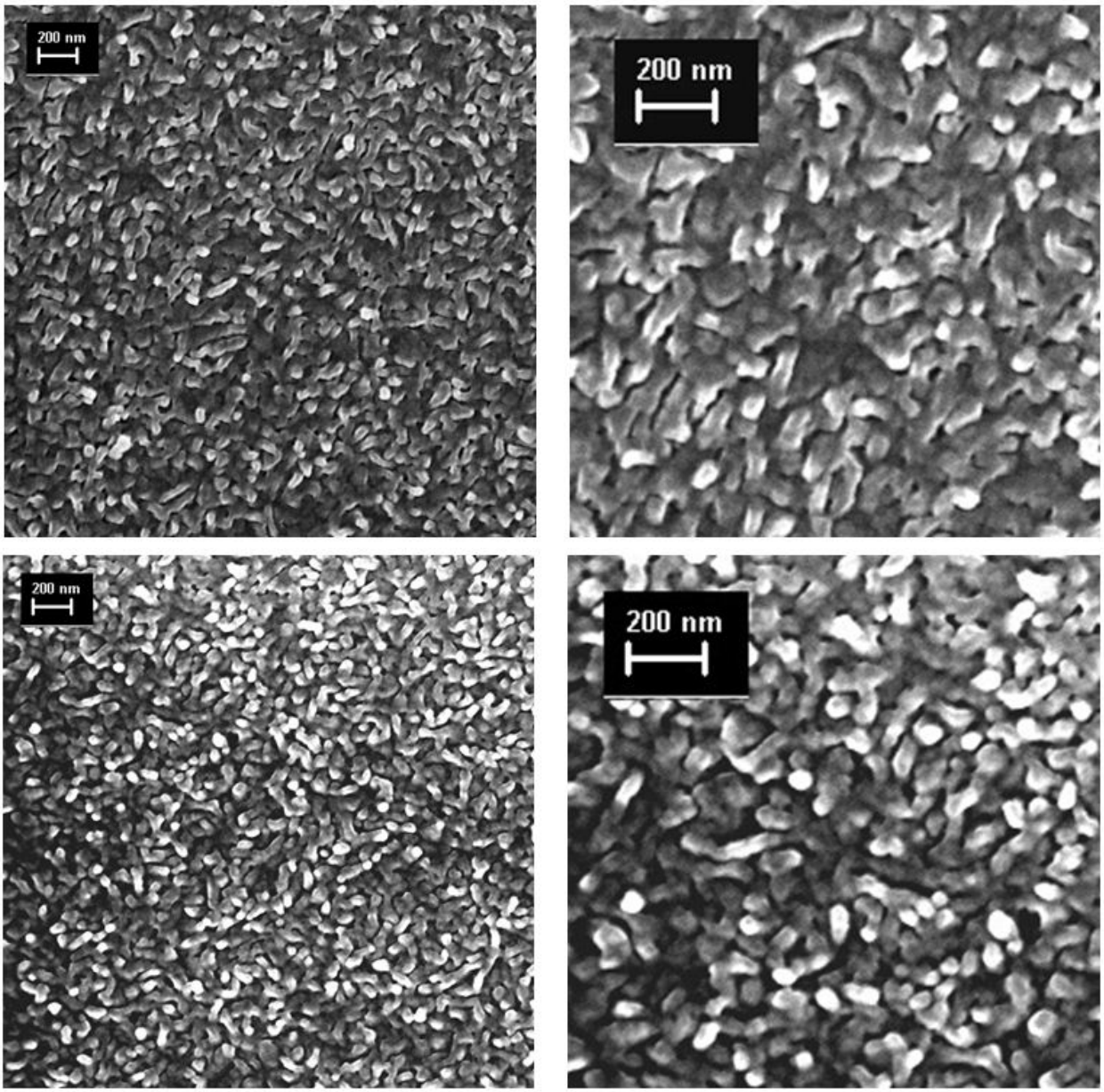

Figure 11.2: The SEM pictures of the Al base electrode shows long crystallites protruding from the surface. The pictures in the top row are taken from a non-heated sample, the images in the lower row from a sample subjected to a 1 h heat treatment.

The microscopic surface area can be assumed to be signifcantly higher than the macroscopic electrode area given by the form of the evaporation mask and to result in a much lower nanoscale base thickess than the evaporated 25 nm. In 9, the different performance of two devices built in one batch is attributed to shadow effects occuring at the evaporation of the base electrode. This explanation is affirmed by the SEM picture shown above - evaporation at angles deviating from 90 ° can be assumed to effect the layer structure. The threedimensional structure may influence the growth and form of the metal layer heavily, rather leading to a threedimesional Al network of inhomogenious thickness than to the twodimensional flat metal sheet depicted in the simplified device sketches. Similar observations in case of vacuum thermal evaporation on a rough crystalline surface have been reported in 2004 by M. Shtein, the formation of voids at the base of protuding

crystals is depicted [43].

Thus, the highly crystalline and rough collector layer may form by itself an inhomogenious base electrode just by shadow-mask evaporation, while on relatively flat organic layers as obtained by spincoating of polymers, the same effect has to be forced by intentional roughening of the surface with polystyrene spheres or by use of a grid-forming base material [1, 18]. Based on this assumption, the electric field cannot be imagined as homogenious as for a flat electrode, the unique morphology would lead to irregularities like spikes and could thereby contribute to the working mechanism.

Additionally, the whole device is investigated by SEM images of the cross section. Pictures of a heated (right hand side) and a not heated device (left hand side) are shown in fig. 11.3. The layers can be clearly identified, the black horizontal stripes resemble the MePTCDI layers (collector at the bottom, emitter on top) and are separated by a thin light grey line (Al base electrode). Again, the roughness of the base electrode in comparison to its thickness is remarkably high. The white circles mark areas of extraordinarily inhomogenious aluminium.

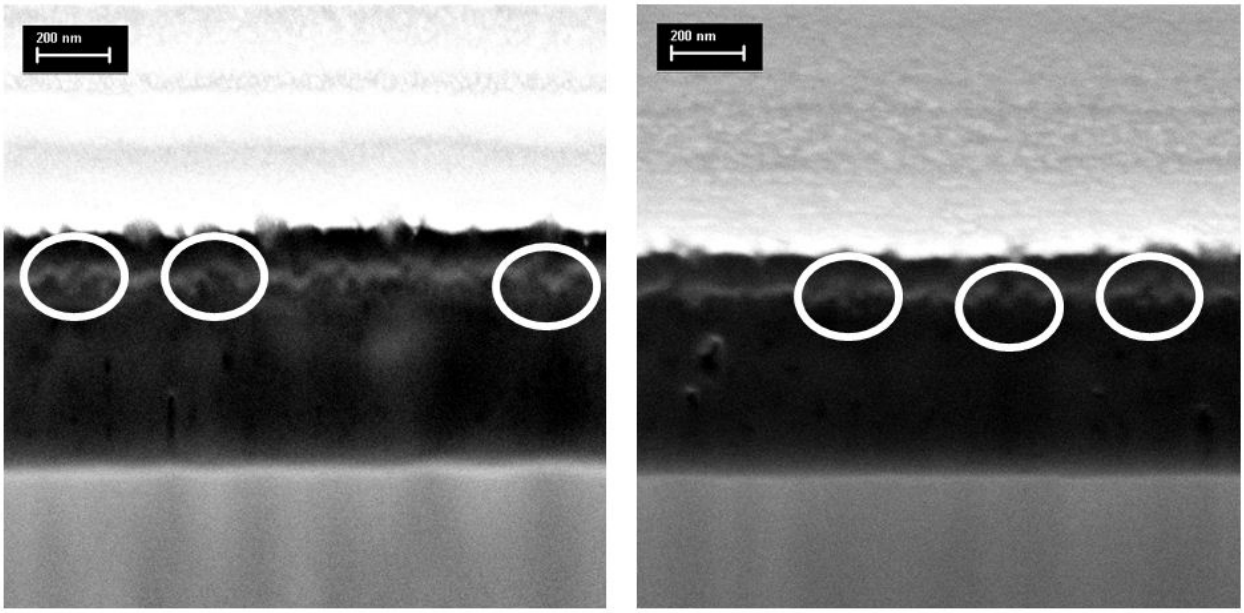

Figure 11.3: The SEM cross section of a full device is shown. The light grey line separating the black stripes depicts the Al base electrode embedded between two MePTCDI layers, the grey area at the bottom is the Si substrate, the bright area on top is the surface of the silver emitter electrode. White circles mark noticable irregularities in the base electrode. Left picture is taken from a non-heated sample, right picture from a sample subjected to 1 h heat treatment.

Many experiments have shown so far the crucial importance of the base electrode to the performance of VOTs with both permeable and non-permeable base electrodes. For PBTs, especially the intenional introduction of holes into the base layer leads to promising results [1, 18]. According to literature, the base transport factor decreases with increasing base thickness in PBT devices using copper phthalocyanine both as emitter and collector and aluminium as base [42]. The thinner the base electrode, the smaller is the current loss due to recombination and the more pinholes are present to allow electron transfer. For MBTs, too, the base electrode is chosen thinnest possible to build

a workable device and to minimize the base current [20]. However, percolation has to be achieved in case of both PBTs and MBTs to allow voltage application, thus defining the minimum thickness needed for a workable device. To find the thickness of percolation, a resistance measurement during Al evaporation on MePTCDI is done as described previously; the resulting graph is shown in fig. 11.4.

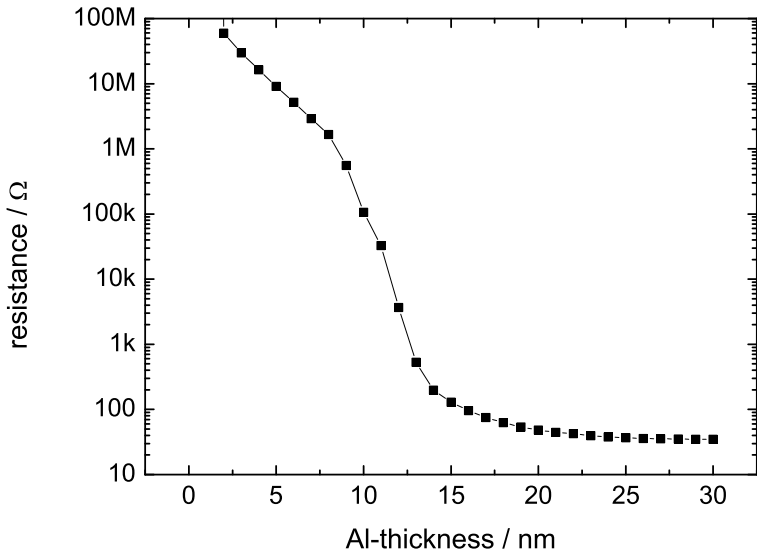

Figure 11.4: The resistance between two Al contacts is measured during evaporation of Al on the underlying MePTCDI, thus the thickness of percolation is found to be around 12 nm.

From the steep decrease of resistance, a percolation thickness of around 12 nm is obtained. Above 20 nm, the resistance decreases very slowly, for 25 nm (the thickness chosen for the base electrode in the devices) a value of 36 Ω is obtained. This indicates again that the metal layer cannot be treated as twodimensional layer because the calculated sheet resistance for the 25 nm thick layer of macroscopically 3.5*8.75 mm^2 differs significantly from the measured value as it gives only 0.53 Ω. As no voltage can be applied to a base electrode consisting of separated islands, the point of percolation gives the minimum base thickness allowing to build a potentially working device. However, the formation of a continuous and hole-free metal layer cannot be obtained from this measurement. The deposition is stopped after 30 nm because no significant changes can be observed for thicknesses higher than 20 nm.

When the heat treatment at air of a half-built device is simulated using the same device, the copper block serving as heater and substrate holder takes 30 minutes to reach 150 °C. While the resistance increases to 55 Ω within the first hour including the heating-up time, the following 1.5 h heating time result only in a further increase of 5 Ω, as shown in fig. 11.5. This flattening of the increase in resistance can be explained when assuming the formation of a continuous protecting oxide layer on top of the aluminium. It is well known in the field of aluminium technology that an aluminium oxide layer built on pristine aluminium or an aluminium magnesium alloy growing at a temperature lower than 300 °C in air reaches a maximum thickness of 1 to 3 nm [44].

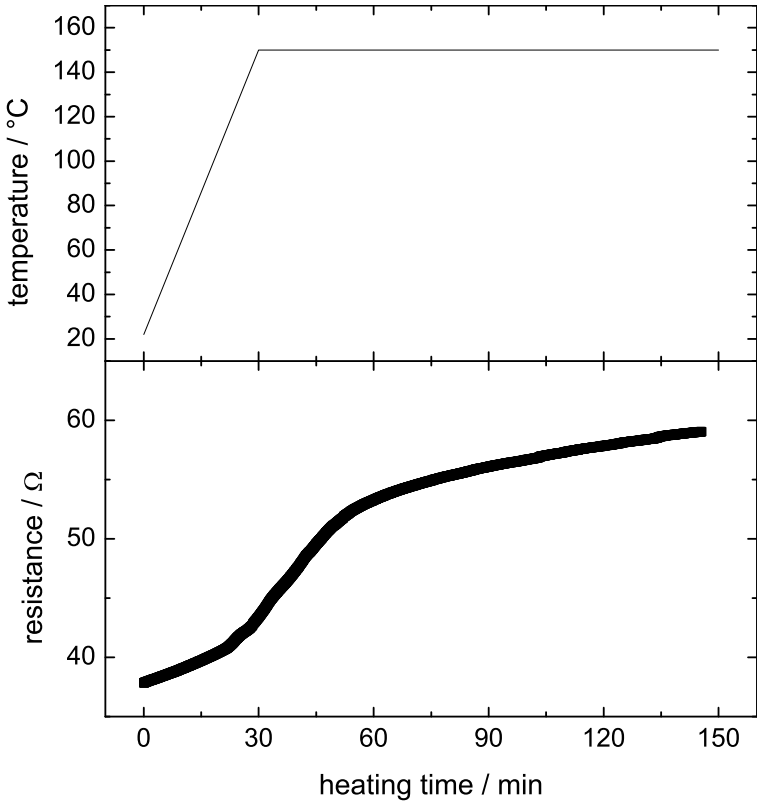

Figure 11.5: The resistance of a 30 nm Al layer on MePTCDI is measured during heat treatment in air, the substrate holder reaches 150 °C after 30 min.

Apart from the formation of an oxide layer on top of the structure, also diffusion of the Al into the semiconductor has to be taken into account. Detailed measurements have been reported for the diffusion of Al into a layer of perylene-3,4,9,10-tetracarboxylic dianhydride PTCDA by H. Yoshida et al. [45]. It is shown that Al does not only diffuse rapidly into PTCDA during its deposition but also at lower rate after evaporation at room temperature. This phenomenon of diffusion is well known from several metal-semiconductor combinations and was also investigated for silver and C_{60} during evaporation and after an annealing step. Applying Fick's law of diffusion for a one-dimensional semi-infinite medium, the diffusion coefficient has an Arrhenius form an is therefore exponentially dependent on the temperature; these calculations fit the measured data very well [37]. The thickness of the deposited Ag layer and the annealing effect the diffusion and therefore conductance of C_{60} significantly. Thus, Sarkar and coworkers expect diffusion to have a great, yet scarcely investigated influence on devices comprising metal- organic semiconductor contacts. Similar experiments are not reported for MePTCDI and Al, yet a similar behaviour might be observed.

While the obtained results for the percolation measurement should be reliable concerning the sample preparation and measurement, the results from the resistance measurement during the heat treatment may be questionable: As mentioned in the experimental part, the wires are brazed onto the pre-deposited contacts, the investigated aluminium layer is evaporated on top of these connections. As the aluminium layer covers the brazed contacts, the oxide layer can be expected to be formed above them, leaving a conducting channel underneath. Thus, the measured increase of resistance

may be attributed solely the formation of an insulating oxide layer but also morphology changes of the threedimensional Al layer may influence the measured resistance. Both explanations cannot be sufficiently confirmed with the obtained data.

The measurement is carried on for two hours after reaching 150 °C and does not show significant resistance changes between one and two hours, this indicates that the aluminium layer is not fully oxidized within this time. In contrast, the characteristics obtained from MePTCDI/C_{60} samples heated for different periods of time differ clearly. Further experiments have to be done to clarify the origin of this behaviour. Explanations may reach from a growing oxide layer, which was not detected properly in the heating experiment above, to nanomorphology changes in the threedimensional collector-base interface reminding of the phase separation observed for annealed solar cells and diffusion processes.

Still, the question arises why the heat treatment increases the performance and reproducibility of the devices. Reported data by Nakayama group and experimental data measured for this work show a more significant decrease in base and off current than in collector current, resulting in improved device parameters [21]. The lowered off current and collector current can be explained sufficiently by the resistance of the oxidation layer which may prevent electrons from crossing the base. Higher reproducibility might be explained by the formation of a nanomorphology which allows more efficient electron transport, as proposed for different types of hybrid and organic vertical transistors.

Electron injection from the emitter into the positively biased base electrode can be sigificantly hindered by an insulating interfacial layer. Assuming openings in the base electrode, electrons can still reach the collector electrode by passing through these voids, thus the base current decreases more significantly than the collector current; better device parameters are obtained. Yet, an oxide layer on top of the base electrode should only have marginal influence on the electrons ejected from the base electrode into the collector - only an insulating layer between base and collector could result in a lowered current between base and collector. Again, changes in the interface morphology and diffusion might be responsible for the observed positive effect, yet more experiments have to be done to propose a sensible explanation.

Part IV

Summary and conclusion

During this work, the production of vertical organic transistors by vacuum thermal evaporation has been proven to result in workable devices. Nevertheless, the samples prepared for this work showed significantly worse parameters such as on/off ratio and current enhancement factor than the published transistors. The positive effect of heat treatment in air mentioned in [23] could be affirmed. As the decrease in off current and base current was more pronounced than the decrease in the on current, the device parameters improved. Additionally, the percentage of workable transistors was found to be greater for batches subjected to a 1 h heat treatment.

In comparison to published C_{60}/MePTCDI devices subjected to a heat treatment in air, the pure MePTCDI devices prepared for this work turn out to operate nearly identically at lower voltages. While the transistors reported in [21] show the maximum current enhancement factor of 150 and a collector current of about 100 mA cm^{-2} at 7 V collector voltage and 3 V base voltage, the transistors presented in this work exhibit a current enhancement factor greater than 150 at 4 V collector voltage for base voltages up to 1.5 V, a maximum value of nearly 500 is reached at 0.75 V; the maximum collector current is measured to be 80 mA cm^{-2}. Thus, simplified devices comprising only one semiconductor material (MePTCDI) as emitter and collector layer were found to exceed the performance of transistors containing a C_{60} emitter. Additionally, workable devices comprising emitter electrodes out of Al and Cr, exhibiting work functions of 4.3 and 4.5 eV, were built. The significant differences in the performance of nominally identical devices complicated the comparison of devices built in different batches.

Data obtained from a resistance measurement on the base electrode during the heat treatment show a slight increase which may indicate, apart from the formation of an insulating oxide layer, morphology changes in the interface.

AFM pictures were taken from the collector layer serving as substrate for the deposition of the base electrode. Grain-shaped crystallites with a diameter of 100 nm result in a roughness more than twice as high as the metal layer which is evaporated on this surface. SEM measurements performed on the base electrode give a more accurate picture of the morphology as they reveal needle-like crystallites of MePTCDI protruding from the surface. At the evaporation of the base electrode, this rough surface can be assumed to lead to the formation of a threedimensional semiconductor-metal interface with a high surface area instead of the sheet-like electrode depicted in simplified sketches and wellknown from the inorganic metal base transistor. This suspicion was substantiated by a percolation experiment performed during the evaporation of Al on a layer of MePTCDI. As percolation was achieved for a thickness of 12 nm, this indicates again the growth of an inhomogenious metal layer.

To confirm these assumptions, additional experiments and techniques have to be applied in future: While neither AFM nor SEM could help to identify voids or pinholes in the metal base, refined techniques such as conductive AFM or XPS might exclude or confirm the existence of openings in the base electrode. Thus, the devices can be identified either as hot-electron transistors or as PBTs. To minimize shadow effects, rotation of the substrate holder during evaporation is suggested. This can be assumed to have a negative effect on the performance of PBTs as voids should be closed or at least reduced in size. A more uniform layer thickness may also effect hot-carrier transport because the layer thickness must not exceed the mean free path of the carriers. The contrary effect can be achieved by evaporation of the base electrode on tilted substrates, thus shadow effects should be increased.

Another way of receiving smoother or even rougher base electrodes might lie in the preparation of the underlying semiconducting collector layer. Extremely low or high deposition rates may effect the surface morphology and cooling of the substrate during the evaporation may minimize the formation of crystallites and result in a smoother surface. Use of C_{60} and PTCDI derivatives with longer alkyl chains are suggested to obtain different surface morphologies.

Additionally, further investigations on the effect of the heat treatment in air are suggested. Measurements of the changes in the in-plane resistance on top of the base electrode and in the resistance vertically throughout the layer may help to gain information on the growth of the oxide layer. Metal diffusion into the semiconductor and the spacial rearrangement of the threedimensional interface during the heat treatment may be investigated in detail.

References

[1] Y. Yang and A. J. Heeger, "A new architecture for polymer transistors," *Letters to Nature*, vol. 372, pp. 344–346, 1994.

[2] S. ya Fujimoto, K. ichi Nakayama, and M. Yokoyama, "Fabrication of a vertical-type organic transistor with a planar metal base," *Applied Physics Letters*, vol. 87, p. 133503, 2005.

[3] L. de Forest, "Space telegraphy," 1908.

[4] H. Röschlau, *Handbuch der angewandten Impulstechnik.* R. v. Decker's Verlag, 1965.

[5] W. Bitterlich, *Elektronik.* Springer Verlag, 1967.

[6] A. P. Speiser, *Impulsschaltungen.* Springer Verlag, 1967.

[7] S. Dimitrijev, *Understanding Semiconductor Devices.* Oxford University Press, 2000.

[8] S. M. Sze and K. K. Ng, *Physics of Semiconductor Devices.* Wiley-Interscience, 2007.

[9] L. L. Liou, B. Bayraktaroglu, and C. I. Huang, "Theoretical thermal runaway analysis of heterojunction bipolar transistors: Junction temperature rise threshold," *Solid State Electronics*, vol. 39, pp. 165–172, 1996.

[10] J. E. Lilienfeld, "Amplifier for electric currents," 1932.

[11] M. Atalla and D. Kahng, "A new 'hot electron' triode structure with semiconductor-metal emitter," in *Solid-State Device Research Conference*, 1962.

[12] M. S. Meruvia and I. A. Hümmelgen, "Hybrid molecular/inorganic semiconductor transistors in vertical architectures," *Advanced Functional Materials*, vol. 16, pp. 459–467, 2006.

[13] E. Rasencher, P. A. Badaz, J. C. Pfister, F. A. d'Avitaya, G. Vincent, and S. Delagea, "Study of ballistic transport in si-cosi2-si metal base transistors," *Applied Physics Letters*, vol. 49, pp. 271–273, 1986.

[14] Z. Bao and J. Locklin, eds., *Organic Field-Effect Transistors.* CRC Press, 2007.

[15] M. Yi, J. Huang, D. Maa, and I. A. Hümmelgen, "Large current gain and low operational voltage permeable metal-base organic transistors based on au/al double layer metal base," *Organic Electronics*, vol. 9, pp. 539–544, 2008.

[16] J. Serbena, J. Huang, D. Ma, Z. Wang, and I. Hümmelgen, "Vertical structure permeable-base hybrid transistors based on multilayered metal base for stable electrical characteristics," *Organic Electronics*, vol. 10, pp. 357–362, 2009.

[17] M. S. Meruvia, A. R. V. Benvenho, I. A. Hümmelgen, A. A. Pasa, and W. Schwarzacher, "Pseudo-metal-base transistor with high gain," *Applied Physics Letters*, vol. 86, p. 263504, 2005.

[18] Y.-C. Chao, H.-F. Meg, and S.-F. Horng, "Polymer space-charge-limited transistor," *Applied Physics Letters*, vol. 88, p. 223510, 2006.

[19] J. Huang, M. Yi, D. Ma, and I. A. Hümmelgen, "Vertical structure p-type permeable metal-base organic transistors based on n,n'-diphentyl-n,n'-bis(1-naphthylphenyl)-1,1'-biphenyl-4,4'-diamine," *Applied Physics Letters*, vol. 92, p. 232111, 2008.

[20] Y.-C. Chao, S.-L. Yang, and H.-F. Meng, "Polymer hot-carrier transistor," *Applied Physics Letters*, vol. 87, p. 253508, 2005.

[21] K. ichi Nakayama, S. ya Fujimoto, and M. Yokoyama, "Improvement in the on/off ratio of a vertical-type metal-base organic transistor by heat treatment in air," *Organic Electronics*, vol. 10, pp. 543–546, 2009.

[22] K. ichi Nakayama, S. ya Fujimoto, and M. Yokoyama, "High-current and low-voltage operation of metal-base organic transistors with lif/al emitter," *Applied Physics Letters*, vol. 88, p. 153512, 2006.

[23] K. Yutani, S. ya Fujimoto, K. ichi Nakayama, and M. Yokoyama, "Role of oxidation layer of aluminum base electrode in metal-base organic transistors," *Molecular Crystals and Liquid Crystals*, vol. 462, pp. 51–57, 2007.

[24] F. Suzuki, K. ichi Nakayama, Y.-J. Pu, and J. Kido, "Current enhancement in the vertical-type metal-base organic transistors," *Molecular Crystals and Liquid Crystals*, vol. 504, pp. 133–139, 2009.

[25] L. Ma and Y. Yang, "Unique architecture and concept for high-performance organic transistors," *Applied Physics Letters*, vol. 85, pp. 5084–5086, 2004.

[26] S.-H. Li, Z. Xu, G. Yang, and Y. Yang, "Solution-processed poly(3-hexylthiophene) vertical organic transistor," *Applied Physics Letters*, vol. 93, p. 213301, 2008.

[27] Z. Xu, S.-H. Li, L. Ma, G. Li, and Y. Yang, "Vertical organic light emitting transistor," *Applied Physics Letters*, vol. 91, p. 092911, 2007.

[28] T. Oekermann and D. Schlettwein, "Characterization of n,n'-dimethyl-3,4,9,10-perylenetetracarboxylic acid diimide and phthalocyaninatozinc(ii) in electrochemical photovoltaic cells," *Journal of Applied Electrochemistry*, vol. 27, pp. 1172–1178, 1997.

[29] H. Hoppe and N. S. Sariciftci, "Organic solar cells: An overview," *Journal of Material Research*, vol. 19, pp. 1924–1945, 2004.

[30] H. Graaf, W. Michaelis, G. Schnurpfeil, N. Jaeger, and D. Schettwein, "Consequences of twisting the aromatic core of n,n'-dimethylperylene-3,4,9,10-biscarboximide by chemical substitution for the electronic coupling and electric transport in thin films," *Organic Electronics*, vol. 5, pp. 237–249, 2004.

[31] D. R. Lide, ed., *CRC Handbook of Chemistry and Physics 82nd edition.* CRC Press, 2001-2002.

[32] N. S. Sariciftci, D. Braun, C. Zhang, V. I. Srdanov, A. J. Heeger, G. Stucky, and F. Wudl, "Semiconducting polymer-buckminsterfullerene heterojunctions: Diodes, photodiodes and photovoltaic cells," *Applied Physics Letters*, vol. 6, pp. 585–587, 1992.

[33] D. Mühlbacher, "Comparative study of the electrochemical and the optical band gap of organic semiconductors," Master's thesis, Johannes Kepler Universität Linz, 2002.

[34] C. Brabec, V. Dyakonov, and U. Scherf, eds., *Organic Photovoltaics: Materials, Device Physics, and Manufacturing Technologies*. Wiley-VCH, 2008.

[35] Y. Kim, S. A. Choulis, D. Nelson, D. D. C. Bradley, S. Cook, and J. R. Durrant, "Device annealing effect in organic solar cells with blends of regioregular poly(3-hexylthiophene) and soluble fullerene," *Applied Physics Letters*, vol. 86, p. 063502, 2005.

[36] F. Padinger, R. S. Ritterberger, and N. S. Sariciftci, "Effects of postproduction treatment on plastic solar cells," *Advanced Functional Materials*, vol. 13, pp. 85–88, 2003.

[37] D. Sarkar and N. J. Halas, "Diffusion of silver in c60 thin films," *Applied Physics Letters*, vol. 63, pp. 2438–2440, 1993.

[38] M. Egginger, S. Bauer, R. Schwödiauer, H. Neugebauer, and N. S. Sariciftci, "Current versus gate voltage hysteresis in organic field effect transistors," *Monatshefte der Chemie*, vol. 140, pp. 735–750, 2009.

[39] P. Stadler, A. M. Track, M. Ullah, H. Sitter, G. J. Matt, G. Koller, T. B. Singh, H. Neugebauer, N. S. Sariciftci, and M. G. Ramsey, "The role of the dielectric interface in organic transistors: A combined device and photoemission study," *Organic Electronics*, vol. 11, pp. 207–211, 2010.

[40] Y. Yang, J. Ouyang, L. Ma, R. J.-H. Tseng, and C.-W. Chu, "Electrical switching and bistability in organic/polymeric thin films and memory devices," *Advanced Functional Materials*, vol. 16, pp. 1001–10014, 2006.

[41] J. He, L. Ma, J. Wu, and Y. Yang, "Three-terminal organic memory devices," *Journal of Applied Physics*, vol. 97, p. 064507, 2005.

[42] S.-S. Cheng, C.-Y. Yang, Y.-C. Chuang, C.-W. Ou, M.-C. Wu, S.-Y. Lin, and Y.-J. Chan, "Influence of thin metal base thickness on the performance of cupc vertical organic triodes," *Applied Physics Letters*, vol. 90, p. 153509, 2007.

[43] F. Yang, M. Shtein, and S. R. Forrest, "Controlled growth of a molecular bulk heterojunction photovoltaic cell," *Nature Materials*, vol. 4, pp. 37–41, 2005.

[44] F. Ostermann, *Anwendugstechnologie Aluminium*. Springer, 2007.

[45] H. Yoshida and N. Sato, "Aluminum diffusion and reaction in thin films of perylene-3,4,9,10-tetracarboxylic dianhydride: Depth profiles and time-dependent diffusion coefficients," *Applied Physics Letters*, vol. 91, p. 141915, 2007.